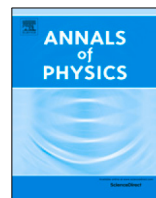




ELSEVIER

Contents lists available at ScienceDirect

Annals of Physics

journal homepage: www.elsevier.com/locate/aop

Slepian eigenvalues as tunnelling rates

Stephen C. Creagh^{a,*}, Gabriele Gradoni^{a,b}^a School of Mathematical Sciences, University of Nottingham, Nottingham NG7 2RD, UK^b Department of Electrical Engineering, University of Nottingham, Nottingham NG7 2RD, UK

ARTICLE INFO

Article history:

Received 8 November 2022

Accepted 21 December 2022

Available online 26 December 2022

Keywords:

Tunnelling

WKB

Slepian

Holographic

MIMO

Communication

ABSTRACT

We calculate the eigenvalues of an integral operator associated with Prolate Spheroidal Wave Functions (or Slepian functions) by interpreting them as tunnelling probabilities in an analogous quantum problem. Doing so allows us to extend a well-known approximation due to Slepian so that it applies outside an important transition region where these eigenvalues pass from being near unity to being near zero. Study of the eigenvalues has traditionally been associated with problems arising in signal analysis and optics but have more recently found relevance in quantifying the channel strengths available to Multiple-In Multiple-Out (MIMO) radio communication. The approach presented promises easier generalisation to the broader range of geometries possible in the latter context.

© 2022 The Author(s). Published by Elsevier Inc. This is an open access article under the CC BY license

(<http://creativecommons.org/licenses/by/4.0/>).

1. Introduction

The eigenvalue problem of the integral operator \hat{K} defined by

$$\hat{K}\psi(x) = \int_{-1}^1 \frac{\sin k(x-x')}{\pi(x-x')} \psi(x') dx', \quad (1)$$

where k is a nonnegative real constant, has been extensively studied in the context of signal analysis, rooted particularly in the pioneering work of the Bell Labs group in [1–8] (see also [9–11] for overviews from a more recent perspective). There it arises out of a problem of optimising the extent to which signals that are band-limited in frequency can also be localised within a fixed time interval. A physically distinct motivation has come from its relevance to the problem of localising

* Corresponding author.

E-mail addresses: stephen.creagh@nottingham.ac.uk (S.C. Creagh), gabriele.gradoni@nottingham.ac.uk (G. Gradoni).

modes within open optical resonators and to diffraction-limited imaging [4,7,12–15]. Related to this second context particularly, this problem has gained new relevance as it, and variations of it, are also central to understanding fundamental aspects of wireless communications by MIMO (Multiple-Input-Multiple-Output) arrays [14,16–19]. In this paper we argue that the problem can usefully be studied in the form of an analogue problem of finding tunnelling probabilities for a particular Hamiltonian in quantum mechanics. This quantum-mechanical perspective allows easy generalisation of the solutions to deformed integral operators that are more pertinent to radio communication and also leads to approximations for the eigenvalues of \hat{K} that significantly extend classical results in the literature.

We argue in particular that the eigenvalues of \hat{K} can be interpreted as tunnelling probabilities of an associated one-degree-of-freedom quantum Hamiltonian \hat{H} and, from this viewpoint, a range of approximate results become available using the properties of both real and complex orbits of the classical analogue $H(x, p)$ [20,21]. These approximations arise in a semiclassical limit where we identify $\hbar = 1/k \rightarrow 0$. In fact, we can exploit standard uniform approximations of tunnelling near hyperbolic fixed points in phase space [22,23] to reproduce in detail an important transition where the eigenvalues of \hat{K} go from being near unity to being near zero. This provides an estimate of the tunnelling probability in terms of the imaginary action of a complex periodic orbit of $H(x, p)$. By approximating this action as a linear expansion in energy around a critical value, we can reproduce a well known result due to Slepian [6]. Moreover, by using the imaginary action without further approximation, we arrive at a description that is valid over a wider range of parameters than Slepian's, but reduces to Slepian's approximation near the transition itself. In this way we can by a single calculation bridge the gap between an approximation by Fuchs [24] that is valid for lower-order eigenvalues near unity, across the transition treated by Slepian, to an approximation due to Widom [25] of higher-order eigenvalues as they approach zero (and see [26] for a more recent improvement of this).

Furthermore, the quantum analogue problem offers a promising route to generalising some of the geometrical characteristics of the treated integral operator. In the quantum mechanical context, the operator defined by (1) can be interpreted as an operator projecting onto a square patch on phase space, with the corresponding classical symbol being at leading order a function that takes the value 1 inside the square and 0 outside it. Projection onto the square is achieved by first projecting onto an interval of the position coordinates and then onto an interval of the momentum coordinate. In the context of MIMO communication, we are interested in projection along more general curvilinear coordinate lines in phase space. The approach taken here points to a generalisation of the accompanying differential operator used to characterise eigenfunctions, and therefore to a generalisation of the tunnelling approximation used to approximate eigenvalues. Note that this generalisation is distinct from the one offered by Daubechies in [27], which is also based around an interpretation of the integral operator as projection onto a region of phase space. There one generalises by specifying the accompanying differential operator, but here the differential operator is derived from the geometry, which, in taking the form of successive projections along coordinate intervals, is closer to the context needed for MIMO communication.

The methodology that we introduce, and the results that we achieve, are important in the emerging field of electromagnetic communication theory (EIT), where communications are carried out by continuous-aperture MIMO (CAP-MIMO) systems [28], including reconfigurable intelligent surfaces (RIS) [29] as well as holographic antennas [30–32]. In this context, it is important to quantify the degrees of freedom for channel diversity [33], as well as to determine optimal patterns for excitation of the surfaces while operating within a specific environment. It is foreseen that surface technologies constitute important enablers for beyond-5G/6G mobile communication networks [34], where the complexity of the propagation environment is embraced and transformed into a resource/service [35].

We conclude this introduction by providing an outline of the paper. In Section 2 we summarise the essential elements of MIMO communication that motivate study of the integral operator (1). In Section 3 we review the essential properties of Slepian functions needed later to derive the approximation based on tunnelling and discuss also how these properties, and particularly the accompanying differential operator, can be deformed towards the skewed geometries pertinent

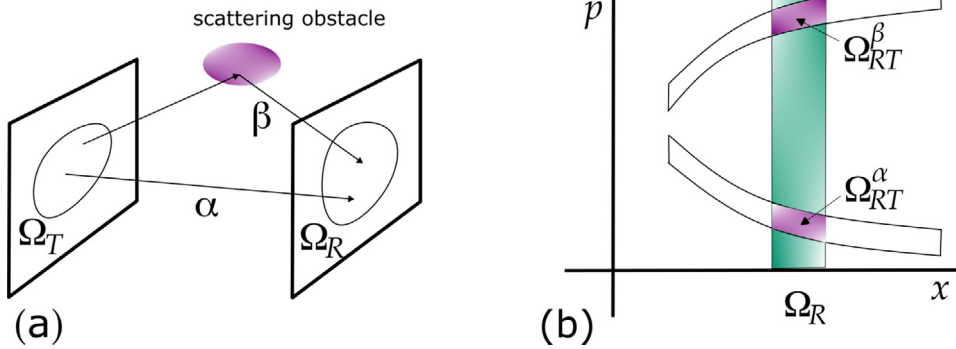


Fig. 1. A schematic illustration of the geometry motivating the study of (1) in this paper. On the left we suppose transmitting and receiving antennae respectively filling surface patches Ω_T and Ω_R . Communication between them may be either Line-of-Sight or by scattering from obstacles. In a corresponding phase-space representation, illustrated in part (b), each topologically distinct path in a far-field scenario defines a patch whose shape is approximately a parallelogram. Communication channels can be defined using a suitable generalisation of (1) to the geometry of these intersections.

to MIMO applications. In Section 4 this differential operator is recast as a quantum analogue problem and a treatment of it within semiclassical approximation (corresponding to the limit $k \rightarrow \infty$) is provided in Section 5. In Section 6 this semiclassical approach is exploited to provide an approximation of the eigenvalues of (1) and to interpret them as tunnelling probabilities. This approximation is evaluated for a model MIMO geometry in Section 7 and compared both with exact results and with limiting approximations from the classical literature. Finally we conclude the paper in Section 8.

2. Motivation for the integral equation and its generalisations from MIMO communication

We are motivated to study the integral operator (1) by its relevance to the problem of calculating communication rates between large arrays of transmitting and receiving antennae in a Multiple-Input-Multiple-Output (MIMO) set up. We focus on a holographic analysis here, where we suppose that antennae are sufficiently densely packed that a continuum model of the resulting surface currents can be used to determine optimal communication channels and their signal strengths for a given physical environment. The problems of bounding communication rates then becomes one that is tackled by assessing related volumes or areas in phase space.

2.1. Essentials of communication

Standard models of communication [18] are based on a relation of the form

$$\mathbf{y} = \mathcal{H}\mathbf{x} + \mathbf{n},$$

between transmitting antenna signals $\mathbf{x} = (x_1, \dots, x_{N_T})^T$ and receiving antenna signals $\mathbf{y} = (y_1, \dots, y_{N_R})^T$, where N_T and N_R are respectively the numbers of transmitting and receiving antennae, the components of $\mathbf{n} = (n_1, \dots, n_{N_R})^T$ are the noise levels experienced by the receiving antennae and \mathcal{H} is an $N_R \times N_T$ transfer matrix. The signal vectors here are characterised by a correlation matrix, denoted

$$\mathcal{R}_T = \frac{1}{P} \langle \mathbf{x}\mathbf{x}^\dagger \rangle, \tag{2}$$

where P is a suitably scaled signal power. It is furthermore commonly assumed that the noise is normally distributed according to

$$\mathbf{n} \sim \mathcal{N}(0, \mathcal{C})$$

and the correlation matrix \mathcal{C} defines a matrix

$$\mathcal{R}_R = \sigma^2 \mathcal{C}^{-1}$$

complementing \mathcal{R}_T at the receiving end, where σ denotes a noise strength and P/σ^2 is a signal-to-noise ratio.

We can assess achievable communication data-rates in this scenario by optimising the *mutual information* [36, Eq. (12)]

$$I = \log_2 \det \left(I + \frac{P}{\sigma^2} \mathcal{H} \mathcal{R}_T \mathcal{H}^\dagger \mathcal{R}_R \right)$$

with respect to \mathcal{R}_T to yield a *channel capacity* C (measured in units of bits/Hz/sec). In particular, we can associate individual channels and their strengths as corresponding respectively to eigenvectors and eigenvalues of the matrix

$$\mathcal{M} = \mathcal{H} \mathcal{R}_T \mathcal{H}^\dagger \mathcal{R}_R. \tag{3}$$

Denoting the eigenvalues of \mathcal{M} by λ_n we can write

$$C = \sum_{n=1}^{N_R} \log_2 \left(1 + \frac{P}{\sigma^2} \lambda_n \right)$$

(\mathcal{M} is similar to the Hermitian matrix $\sqrt{\mathcal{R}_R} \mathcal{H} \mathcal{R}_T \mathcal{H}^\dagger \sqrt{\mathcal{R}_R}$ and so its eigenvalues λ_n are real). Although more general formulations are possible, a common special case is that the matrices $\mathcal{R}_{T,R}$ are identity matrices of appropriate rank:

$$\mathcal{R}_T = I_{N_T \times N_T} \quad \text{and} \quad \mathcal{R}_R = I_{N_R \times N_R}. \tag{4}$$

Then the eigenvalues λ_n are simply squares of the singular values of the transfer matrix \mathcal{H} and its rank determines the number of communication channels available to the system.

2.2. The holographic model: towards a continuum picture

As MIMO systems evolve towards increasingly dense antenna arrays, a holographic picture, in which we suppose we can control surface currents with unlimited spatial resolution rather than assuming discrete antennae, is increasingly relevant; that is, the transmit/receive array is approximated as a continuous (holographic) surface [33]. It is important to understand the effective degrees of freedom of such dense surfaces, as this constitutes a fundamental limit for field sampling [37,38]. For such dense/continuous surfaces, the matrix \mathcal{M} defined in (3) is replaced by an integral operator very similar in form to (1), as we now outline. We first present the more general picture in broad outline and then write down more concretely in Section 2.3, albeit in a much simplified and restricted setting, an idealised problem which aims to capture the essential features required for a generalisation of (1) towards this broader problem.

In particular, we replace in the holographic formulation the correlation matrices \mathcal{R}_T and \mathcal{R}_R by two-point field-field correlation functions

$$\mathcal{R}_{T,R} \rightarrow \Gamma_{T,R}(x_1, x_2) = \langle \psi(x_1) \psi^*(x_2) \rangle_{T,R},$$

in which functions $\psi(x)$ of continuous boundary coordinates x replace the discrete signal levels \mathbf{x} and \mathbf{y} . We confine the transmitting and receiving antennae to surface patches denoted Ω_T and Ω_R respectively (see the schematic illustration in Fig. 1), so that we constrain the correlation functions $\Gamma_T(x_1, x_2)$ and $\Gamma_R(x_1, x_2)$ to be supported on these sets.

Let d denote the dimension of these boundary sets. We should clearly set $d = 2$ to fully model a physical, 3D MIMO system, but in the following we examine simplified calculations in which $d = 1$, which is also the setting of (1). A particularly important special case is where these correlation functions take the form of spatially white noise, of the forms

$$\Gamma_{T,R}(x_1, x_2) = \delta(x_1 - x_2) \chi_{T,R}(x_1), \tag{5}$$

where $\chi_T(x)$ and $\chi_R(x)$ respectively denote the characteristic functions of the patches Ω_T and Ω_R . In fact, these provide integral kernels for corresponding operators defined by multiplication

$$\hat{T}_{T,R} : \psi(x) \mapsto \chi_{T,R}(x)\psi(x).$$

These special cases provide the continuum analogues of the correlation matrices in (4), up to a scaling factor.

We suppose that the signal amplitude $\psi_R(x)$ arriving at Ω_R after emission from source $\psi_T(x)$ in Ω_T can be expressed in the form

$$\psi_R = \hat{T}\psi_T$$

where \hat{T} is a transfer operator

$$\psi_R(x) = \int_{\Omega_T} T(x, x')\psi_T(x')dx',$$

with a kernel $T(x, x')$ that is commonly approximated semiclassically as a sum over ray paths from Ω_T to Ω_R . The detailed form given for $T(x, x')$ depends on the physical formalism used to model transmitted and received signals. A common physical description uses surface currents for $\psi_T(x)$ and potentials for $\psi_R(x)$: in this case $T(x, x')$ is simply a Green function, whose approximation in terms of ray paths is well established [39]. An alternative that is particularly convenient for our analysis is to locally scale transmitted and received signals so that they are on an equal footing, and connected by a transfer operator of the kind described semiclassically by the formalism in [40]. The transfer operator \hat{T} is the continuum analogue of the transfer matrix \mathcal{H} . Then the holographic analogue of (3) is the operator

$$\hat{\varrho} = \hat{T}\hat{T}_T\hat{T}^\dagger\hat{T}_R. \tag{6}$$

We now argue that the action of $\hat{\varrho}$ generalises (1) (up to a cyclic permutation of operators).

In the corresponding ray-dynamical phase space, in which boundary coordinates x are augmented by momentum coordinates p determining the direction cosines of the corresponding ray, we use an abuse of notation to let the symbols $\Omega_{R,T}$ also denote the vertical strips defined by $x \in \Omega_{R,T}$. Let φ denote the mapping in phase-space coordinates (x, p) from the part of the boundary containing Ω_T to the part containing Ω_R . Then the geometry of the intersections

$$\Omega_{RT} = \Omega_R \cap \varphi\Omega_T \quad \text{and} \quad \Omega_{TR} = \varphi^{-1}\Omega_{RT} = \varphi^{-1}\Omega_R \cap \Omega_T$$

are key to understanding the operator in (6). Note that in a typical multipath scenario, each of these intersections may be composed of discrete components Ω_{RT}^α (or alternatively Ω_{TR}^α) defined by topologically distinct paths α as illustrated in Fig. 1. The detailed connection between $\hat{\varrho}$ and the patches Ω_{RT}^α is made by approximating \hat{T} in the high-frequency limit as a sum over paths α connecting Ω_T to Ω_R [39,40], so that $\hat{\varrho}$ becomes in turn a double sum over such paths. Diagonal contributions, in which the path connecting Ω_R to Ω_T by \hat{T}^\dagger is a reversal of the path α connecting Ω_T to Ω_R by \hat{T} , are associated with the intersection patches Ω_{RT}^α . Establishing this connection in detail is an interesting topic for future work but is complicated by aspects such as the control of errors and the effect of interference arising from nondiagonal contributions to the double sum over paths. We put these issues aside in the next section by restricting our attention to a very simplified model which we hope nevertheless captures the essential elements of the more general scenario.

2.3. An idealised holographic model

The operator in (6) is a significantly more complicated object in its full generality than the operator in (1). We consider an idealised model which simplifies (6) in two important respects.

First, $\hat{\varrho}$ should act on patches of dimension $d = 2$ in a completely physical model, while the operator \hat{K} acts on patches of dimension $d = 1$. While extensive investigations have been made that generalise (1) to higher dimensions, we choose to focus in this paper on generalisation in a different direction and confine our attention to scalar wave models for which $d = 1$. Our focus is instead on

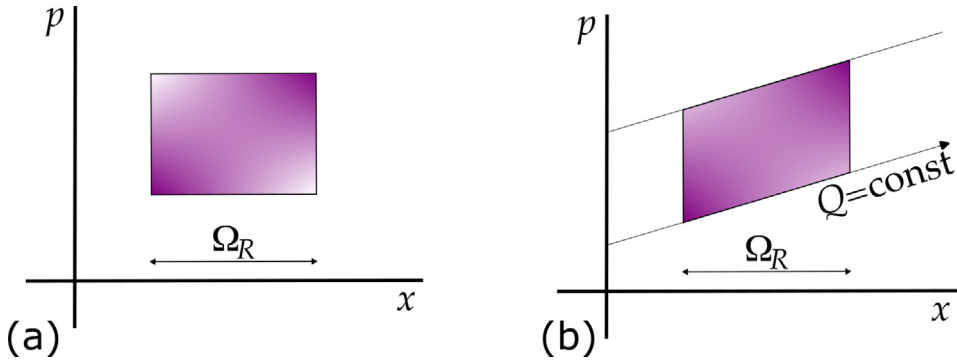


Fig. 2. The integral operator in (1) corresponds to the picture in part (a), in which one sequentially projects vertically and then horizontally in phase space. The local intersections in Fig. 1(b), which correspond to the operator in (6), motivate us to consider a skewed version of this shown in part (b) in which the horizontal projection is replaced by one along a general coordinate Q .

differences arising from the fact that \hat{T} acts more complicatedly than the simple frequency filtering underlying \hat{K} , leading us to generalisations of (1) which have received relatively less attention until now.

The second idealisation is made to avoid complications arising from the fact that \hat{T} is typically used as a semiclassical, small-wavelength approximation. The lengths of the paths α are typically much larger than the width of either Ω_T or Ω_R so that the corresponding intersections in phase space are deformed parallelograms. A treatment of the fully deformed geometry leads to approximate treatments arising from the nonlinear nature of the ray dynamics. We instead restrict our attention to idealised transfer operators whose ray-dynamical analogue is a linear transformation of coordinates (x, p) , and for which the intersection Ω_{RT} is a simple parallelogram with straight edges. The resulting geometry is illustrated in Fig. 2 and the details of the correspondingly-defined integral operator are set out in the next section.

More precisely, we suppose an operator of the form given in (6) in which $\hat{T} \Gamma_T \hat{T}^\dagger$ corresponds in phase space to a patch formed by projection along a coordinate

$$Q = ax + bp, \tag{7}$$

where a and b are real constants. This model is achieved if \hat{T} effectively quantises a linear transformation from (x, p) to new coordinates (Q, P) with Q as given above. The details of this are set out in Section 3.4 and note that in the special case $(Q, P) = (p, -x)$ then \hat{T} becomes a simple Fourier transform and we recover (a scaled, translated version of) (1).

3. Slepian functions: properties and generalisation

We now summarise the most important properties of the eigensolutions of \hat{K} . These are available from a wide range of references (see [10] for example) and we do not give detailed derivations here, but the tunnelling analogue in later sections will provide explanations for key aspects of these.

3.1. A commuting differential operator

The eigenvalue equation

$$\hat{K} \psi_n(x) = \lambda_n \psi_n(x) \tag{8}$$

is solved in the literature by observing that \hat{K} commutes with the differential operator

$$\hat{H} = -\frac{1}{k^2} \frac{d}{dx} (1 - x^2) \frac{d}{dx} + x^2, \tag{9}$$

subject to boundary conditions that the solution is differentiable everywhere on the real line, and in particular at the regular singular points¹ $x = \pm 1$ of the corresponding differential equation [10].

Since these operators commute, they have the same eigenfunctions (but different eigenvalues). We denote the eigenvalues of \hat{H} by E_n , so that the eigenfunctions $\psi_n(x)$ are then also solutions of the differential equation

$$-\frac{1}{k^2} \frac{d}{dx} (1-x^2) \frac{d\psi_n}{dx} + x^2 \psi_n(x) = E_n \psi_n(x). \tag{10}$$

The solutions of this equation are Slepian functions, or prolate spheroidal wave functions (PSWFs), for which there is an extensive literature [10,41]. The original problem is therefore in large part “solved” by the observation of compatibility of \hat{K} with \hat{H} . However, although WKB approaches then provide immediate approximation of the eigenfunctions $\psi_n(x)$ and the eigenvalues E_n of \hat{H} , the eigenvalues λ_n of \hat{K} are less directly available and approximations for them are harder to find. The tunnelling calculations in later sections of this paper help to bridge that gap.

Finally, we note that the detailed calculations in this section are presented for a conventional special case where filtering is on the square patch $(x, p) \in (-1, 1) \times (-1, 1)$, which has an area in phase space of $\mathcal{A} = 4$. More generally, we are interested of course in the case of rectangular patches of arbitrary area \mathcal{A} , centre and aspect ratio. Solutions for the most general case can be obtained from those of the conventional case by scaling and translation operations, and in particular the scaling $k \rightarrow k\mathcal{A}/4$ of the constant k . A similar comment applies to generalisation of these calculations to the skewed case implied by (7). We will assume projection onto a particular interval $Q \in (-1, 1)$ and rely on scaling and translation operations to generalise the derived relationships at the end.

3.2. Fourier transforms of the eigenfunctions

We now select key properties of the PSWFs under Fourier transformation, which will be used later to justify the approximation of λ_n as a tunnelling probability.

Let the Fourier transform operator F be defined by

$$[\hat{F}\psi](p) \equiv \varphi(p) = \sqrt{\frac{k}{2\pi}} \int_{-\infty}^{\infty} e^{-ikxp} \psi(x) dx. \tag{11}$$

Then

$$\hat{F} : \psi_n(x) \mapsto \varphi_n(p) = \frac{i^n}{\sqrt{\lambda_n}} \chi(p) \psi_n(p), \tag{12}$$

where

$$\chi(p) = \begin{cases} 1 & -1 < p < 1 \\ 0 & \text{otherwise} \end{cases} \tag{13}$$

is the characteristic function of the interval $(-1, 1)$. That is, the Fourier transform φ_n of ψ_n is a scaled, band-limited version of ψ_n : they have the complementary properties of being respectively compactly supported and analytic on the real line.

We do not prove this property here, but a discussion can be found in [10,11], for example. This is the key relationship we will use to motivate tunnelling-probability interpretations for the eigenvalues λ_n in later sections.

3.3. Projection operators and the integral equation

Define an operator \hat{L} which projects onto the interval $-1 < x < 1$ as follows

$$\hat{L}\psi(x) = \chi(x)\psi(x),$$

¹ The term *singular point* is used here according to the terminology of differential equations to denote values of x where the coefficient of the second derivative vanishes and where the corresponding differential equation admits solutions that are singular.

where the characteristic function $\chi(x)$ of the interval $(-1, 1)$ has been defined in (13). A second projection operator \hat{M} is defined by the action

$$\hat{M} : \varphi(p) \rightarrow \chi(p)\varphi(p)$$

in Fourier representation, which is equivalent in direct representation to

$$\hat{M} = \hat{F}^\dagger \hat{L} \hat{F}. \tag{14}$$

Then the integral operator \hat{K} defined in (1) can be written

$$\hat{K} = \hat{M} \hat{L}. \tag{15}$$

Evaluating the action of this operator explicitly in direct representation leads to (1).

3.4. A skewed integral operator

We generalise these solutions to account for the skewed geometry illustrated in Fig. 2 by replacing the Fourier transform operator \hat{F} by the following metaplectic operator (see [42] for example)

$$[\hat{T}\psi](Q) \equiv \varphi(Q) = \sqrt{\frac{k}{2\pi}} \int_{-\infty}^{\infty} \left| \frac{\partial^2 F}{\partial Q \partial x} \right|^{1/2} e^{ikF(Q,x)} \psi(x) dx, \tag{16}$$

where

$$F(Q, x) = \frac{1}{2b} (dQ^2 - 2Qx + ax^2)$$

is a generating function satisfying the conditions

$$\frac{\partial F}{\partial Q} = P \quad \text{and} \quad \frac{\partial F}{\partial x} = -p$$

for the linear change of coordinates $(x, p) \rightarrow (Q, P)$ given by

$$\begin{pmatrix} Q \\ P \end{pmatrix} = \begin{pmatrix} a & b \\ c & d \end{pmatrix} \begin{pmatrix} x \\ p \end{pmatrix}, \tag{17}$$

in which $ad - bc = 1$ is assumed so that the transformation is symplectic (area-preserving). Note that the inverse transformation is formed by replacing $F(Q, x)$ with $F(x, Q) = -F(Q, x)$. The operator (16) has been written for a general linear symplectic transformation $(x, p) \rightarrow (Q, P)$ and is useful in this form for later discussion: it can also be used as a basis for generalising the results in this paper to projection onto an arbitrary parallelogram, whose boundaries are defined by constant values of Q and P . In applications to MIMO communication, however, it is always the case that the parallelogram of interest has vertical sides, defined by setting x to constant values. For much of this discussion it then suffices to choose

$$d = 0 \quad \text{and} \quad c = -\frac{1}{b} \tag{18}$$

so that $P = -x/b$ and sides of constant P are also sides of constant x . For this purpose we may also assume without loss of generality in the following that $b > 0$ and let

$$k_b = \frac{k}{b} \tag{19}$$

define a correspondingly scaled wavenumber.

We continue with the properties of \hat{T} in the more general case, as this can be done at little extra cost. Denote corresponding operators

$$\begin{aligned} \hat{Q} &= a\hat{x} + b\hat{p} = ax + \frac{b}{ik} \frac{d}{dx} \\ \hat{P} &= c\hat{x} + d\hat{p} = cx + \frac{d}{ik} \frac{d}{dx}. \end{aligned} \tag{20}$$

Then the relations

$$\begin{aligned} \hat{T}[\hat{Q}\psi(x)] &= Q\varphi(Q) \\ \hat{T}[\hat{P}\psi(x)] &= \frac{1}{ik}\varphi'(Q) \end{aligned}$$

are easily derived from (16) and generalise corresponding derivative relations of the standard Fourier transform. The relation

$$\hat{T}[x\psi(x)] = dQ\varphi(Q) - \frac{b}{ik}\varphi'(Q) \tag{21}$$

is obtained from these by inverting the associated linear transformation of operators. Note that this reduces to

$$\hat{T}[x\psi(x)] = -\frac{1}{ik_b}\varphi'(Q) \tag{22}$$

in the special case noted in (18), which mirrors more closely the corresponding identity for conventional Fourier transforms.

Then we generalise the discussion in Section 3.3 by once again defining an integral operator by (15) except that now the operator \hat{M} is defined by the action

$$\hat{M} : \varphi(Q) \rightarrow \chi(Q)\varphi(Q)$$

on the transform $\varphi(Q)$ of $\psi(x)$ and is written in direct representation as

$$\hat{M} = \hat{T}^\dagger \hat{L} \hat{T}. \tag{23}$$

Working this out explicitly leads to the generalisation

$$\hat{K}\psi(x) = e^{-ik_b a x^2/2} \int_{-1}^1 e^{ik_b a x'^2/2} \frac{\sin(k_b(x-x'))}{\pi(x-x')} \psi(x') dx', \tag{24}$$

of (1), reverting back to it in the special case $\hat{T} = \hat{F}$, for which $a = 0$ and $b = 1$. This more general problem also reverts to (1) after making a gauge transformation $\psi(x) \rightarrow e^{-ikax^2/2}\psi(x)$ and then rescaling $k \rightarrow k_b$. In other words, in order to understand the eigensolutions of (24), it suffices to solve the original problem (1) and perform a simple transformation at the end. Note that this deformation of phase space by a gauge transformation of quadratic phase is also an important element in existing applications of (1) to the study of modes of open optical resonators [12]: We study (24) as a special case of more general metaplectic transformations, however, because it leads more directly to treatments of nonlinear transformations and geometries as follows.

The form given in (16) can be extended to nonlinear changes of coordinate $(x, p) \rightarrow (Q, P)$, generated by functions $F(Q, x)$ that are higher-order than quadratic and correspond to replacing the simple parallelograms in Fig. 2 with projection along more general curvilinear coordinate lines, at the expense of letting the transformation (16) be stated approximately (see [39,43] for more in-depth discussion of such so-called Van Vleck approximations). In particular, we can let Q represent the initial position coordinate of a ray leaving Ω_T and $F(Q, x)$ represent the length of the ray arriving at position x in Ω_R in the more general case. Thus we expect the approach taken here to be applicable to more general problems although we simplify the presentation in this paper by restricting to the linear case.

4. An analogue problem in quantum and classical mechanics

The integral and differential equations of the previous section are converted into analogue quantum problems by making the identification $k \rightarrow 1/\hbar$.

4.1. An analogue quantum Hamiltonian

The generalised integral operator (24) commutes with the differential operator

$$\hat{H} = \hat{Q}(1 - x^2)\hat{Q} + x^2 = \hat{x}^2 + \hat{Q}^2 - \hat{Q}\hat{x}^2\hat{Q}, \tag{25}$$

where \hat{Q} is defined in (20), subject to the conditions that the solution should be differentiable at the singular points $x = \pm 1$ of the corresponding differential equation. The eigenfunctions $\psi_n(x)$ of (24) can then be presented as stationary states of a time-independent Schrödinger equation

$$\hat{H}\psi_n = E_n\psi_n.$$

This Hamiltonian can also be written in the forms

$$\hat{H} = \hat{x}(1 - \hat{Q}^2)\hat{x} + \hat{Q}^2 = \hat{x}^2 + \hat{Q}^2 - \hat{x}\hat{Q}^2\hat{x}, \tag{26}$$

which can be shown using the standard commutation relations between \hat{x} and \hat{p} set out in Appendix A. Even though these expressions are formally symmetrical with respect to exchange of \hat{x} and \hat{Q} , the imposed boundary conditions (that $\psi_n(x)$ is differentiable at $x = \pm 1$) breaks that symmetry. Thus, for example, we find that the integral transform operator \hat{T} defined by (16) does not preserve \hat{H} : the eigenfunction $\psi_n(x)$ and its transform $\varphi_n(Q)$ are distinct. The boundary conditions also explain why the spectrum of \hat{H} is discrete, even though its classical analogue described below is unbounded and can be used to define a scattering problem.

Although the commutation of \hat{H} with \hat{K} has been a standard feature of the treatment of (1) since the early work by the Bell group in [1–5] (and a detailed derivation is provided in [10] for example), we revisit the justification for it in the remainder of this section. We do so first because the necessity of the imposed boundary conditions at $x = \pm 1$ is often taken for granted in the established literature but is not immediately evident in the context of the analogue quantum problems: a more detailed discussion is then useful for the semiclassical treatment coming in Sections 5 and 6. Second, by formulating the boundary conditions as a no-flux condition across appropriate lines in phase space (see Appendix A), we provide a platform for extending the outcome in future to the more general setting outlined at the end of Section 3.4, simply by allowing these bounding lines to become curves. Lastly, although well-established technically, the commutation of \hat{H} with \hat{K} is often not well-motivated in the literature: discussions frequently cite Slepian’s characterisation of it as a “lucky accident” [8], for example. The simple physical intuition offered by the quantum analogue is therefore appealing.

4.2. An analogue classical hamiltonian

In understanding the nature of these stationary states, and in order later to use WKB methods to approximate them, it is helpful to define the corresponding classical Hamiltonian

$$H(x, p) = x^2 + Q(x, p)^2 - x^2Q(x, p)^2. \tag{27}$$

The phase portrait defined by level curves $H(x, p) = E$ of this Hamiltonian is shown in Fig. 3, for both the conventional case $Q = p$ on the left and for a more generic case on the right. Note that the level curves corresponding to $E = 1$ are lines defined by $Q = \pm 1$ and $x = \pm 1$ respectively. This observation provides a simple explanation of the classical analogue of the commutation of \hat{K} and \hat{H} .

Define classical observables

$$L(x, p) = \chi(x)$$

and

$$M(x, p) = \chi(Q),$$

projecting onto the interval $(-1, 1)$ on the x and Q coordinates respectively, and note that

$$K(x, p) = M(x, p)L(x, p) = \chi(x)\chi(Q),$$

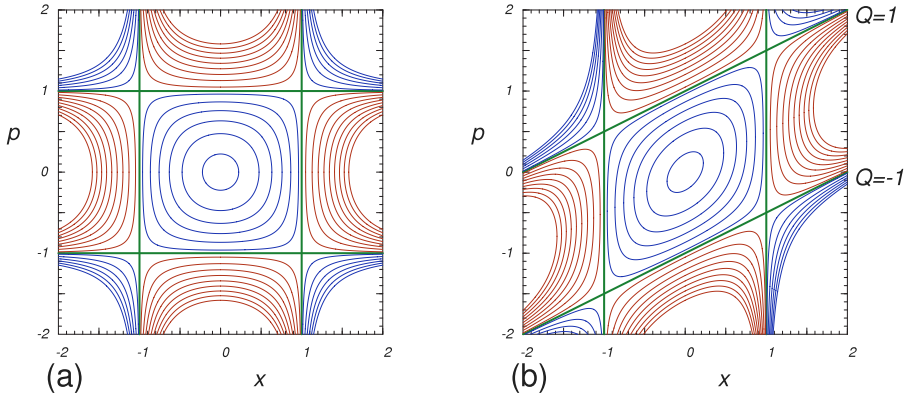


Fig. 3. Phase portrait of the classical Hamiltonian $H(x, p)$, for the conventional square case in part (a) and for a skewed case (in which $a = -1/2$ and $b = 1$) in part (b). The energy contours for $E = 1$ are shown as heavy green lines in each case. Contours for $0 < E < 1$ are shown in blue and contours for $E > 1$ are shown in red.

is the characteristic function of the parallelogram defined by $-1 < x < 1$ and $-1 < Q < 1$. We can interpret $K(x, p)$ as a classical symbol for the integral operator \hat{K} . Then, because the supports of $L(x, p)$, $M(x, p)$ and $K(x, p)$ are bounded by the straight lines $x = \pm 1$ and $Q = \pm 1$, which are also the energy contours $H(x, p) = E$ with $E = 1$, these functions are invariant under the dynamics of $H(x, p)$. That is,

$$\dot{L} = \{L, H\} = 0 \tag{28}$$

and similarly

$$\{M, H\} = 0 = \{K, H\}, \tag{29}$$

where $\{\cdot, \cdot\}$ denotes a Poisson bracket. That is, the classical symbols of \hat{K} and \hat{H} Poisson-commute, which allows us to hope that the operators themselves commute. However, the quantum analogue demands a closer inspection of the boundary conditions imposed.

4.3. Boundary conditions

The commutation of operator \hat{K} with \hat{H} is established as a consequence of the commutation of \hat{H} with \hat{L} . We argue first in the conventional case $Q = p$, for which the integral transform \hat{T} reduces to the conventional Fourier transform \hat{F} , and use that the more general case is obtained from this following a gauge transformation at the end to extend the conclusions. Details are demonstrated in [Appendix A](#) and here we set out the main requirement for this commutation property, which is that boundary conditions are placed on the wavefunction $\psi(x)$ that eliminate singular solutions of the differential Eq. (10). In fact, any eigenfunction of \hat{K} , being the (inverse) Fourier transform of a bandlimited function of p according to (14) and (15), must be analytic on the real line, according to the Paley–Wiener theorem. Such smoothness conditions are therefore natural in the context of solving the corresponding integral equation and are taken for granted in the established literature.

However, from the viewpoint of finding stationary states of a Hamiltonian \hat{H} in the quantum mechanical context, these conditions are less obvious. For example, singular solutions are perfectly physical in closely-related normal-form treatment of quadratic scattering problems [22,23]. Furthermore, these boundary conditions play a central role in breaking the symmetry with respect to interchange of operators \hat{x} and \hat{p} and in leading to a discrete spectrum $\{E_n\}$, even though the Hamiltonian (25) defines an unbound scattering problem for which we might heuristically expect a continuous spectrum in the quantum-mechanical context.

It is shown in [Appendix A](#) that the condition

$$[\hat{L}, \hat{H}]\psi(x) = 0$$

leads to a requirement that $\psi(x)$ be differentiable at $x = \pm 1$. An analysis of the differential Eq. (10) around each of its singular points $x = \pm 1$ using the Frobenius method reveals the independent solutions to be of the forms

$$F(x) \quad \text{and} \quad F(x) \log|x \mp 1| + G(x) \tag{30}$$

respectively, where $F(x)$ and $G(x)$ are analytic there. Imposition of conditions of differentiability therefore eliminates the second of these solutions at each of the two singular points, and explains the resulting discrete spectrum. From the Paley–Wiener theorem, the differentiability condition must in any case hold if $\psi(x)$ is an eigenfunction of \hat{K} , so it is natural from the point of view solely of the integral equation. However, note that the corresponding solution $\varphi(p)$ in momentum representation does *not* satisfy the corresponding differentiability condition around $p = \pm 1$: the Paley–Wiener theorem asserts instead that $\varphi(p)$ is bandlimited. Thus the boundary condition breaks the symmetry of interchange of x and p .

The conditions of differentiability at $x = \pm 1$ are inconvenient to apply to WKB treatments of the solutions, which are at the heart of the discussion in Section 5. This is because a singularity of a WKB approximation does not convert simply to a corresponding singularity of the exact solution. For example, primitive WKB approximations of the conventional Schrödinger equation that are singular near generic turning points are replaced there by smooth, uniform treatments to approximate the correspondingly smooth, exact solutions. For this reason we impose an alternative boundary condition

$$\lim_{p \rightarrow \pm\infty} p\varphi(p) \rightarrow 0 \tag{31}$$

on the Fourier transform $\varphi(p)$ of $\psi(x)$, suggested as a variant of the Riemann–Lebesgue lemma applied to $\psi'(x)$, which avoids this problem. We argue in Section 5.3 that this boundary condition (or its generalised form given in (33) below) must also be satisfied by WKB approximations. This alternative offers a simpler way to impose boundary conditions on the graph model in Section 5 in particular.

We have established conditions for $[\hat{L}, \hat{H}] = 0$, but have not yet concluded that $[\hat{K}, \hat{H}] = 0$. For the latter, use the derivation identity

$$[\hat{K}, \hat{H}] = [\hat{M}\hat{L}, \hat{H}] = \hat{M}[\hat{L}, \hat{H}] + [\hat{M}, \hat{H}]\hat{L}. \tag{32}$$

Now, the image of the operator \hat{L} , being compactly supported in x , consists in momentum representation of analytic functions of p , by the Paley–Wiener theorem. By repeating the argument above, but in momentum representation, and using the formal symmetry of \hat{H} with respect to interchange of the operators \hat{x} and \hat{p} , we can therefore deduce that

$$[\hat{M}, \hat{H}]\hat{L}\psi(x) = 0,$$

regardless of the boundary conditions imposed on $\psi(x)$. We deduce therefore that $[\hat{K}, \hat{H}]$ as expressed in (32) vanishes on the domain of differentiable functions $\psi(x)$.

We finally argue that the previous discussion can be extended to the skewed representation $\varphi(Q)$ resulting simply in

$$\lim_{Q \rightarrow \pm\infty} Q\varphi(Q) \rightarrow 0 \tag{33}$$

replacing (31). This can be achieved by recalling that the skewed problem is obtained by a gauge transformation of the conventional one in order to generalise the parts of the argument invoking Fourier-transform (such as Paley–Wiener and Riemann–Lebesgue) theorems. Furthermore, a physical interpretation of this boundary condition is provided in [Appendix C](#) in terms of flux crossing coordinate lines in phase space. Although the details of the preceding discussion do not easily generalise to the case where these lines become more general curves, this physical interpretation does, so we assert that these boundary conditions have a clear generalisation to the curvilinear case so that the graph-scattering picture in Section 5 remains qualitatively similar.

5. Semiclassical approximation of eigenfunctions and eigenvalues

With boundary conditions in place, we are now in a position to summarise how eigenfunctions $\psi_n(x)$ may be approximated semiclassically, along with the corresponding eigenvalues E_n (in this section) and λ_n (in the next section). These approximations are based on a description of the classical orbits in phase space, including complex solutions so that we can account for coupling by tunnelling between local solutions inside the interval $-1 < x < 1$ and those outside it. For the Hamiltonian (27) these classical solutions can be expressed explicitly in terms of elliptic functions, with details set out in Appendix B, but here in the main text we just summarise the main features.

5.1. Classical solutions and local WKB approximations

Using $H(x, p) = E$ to eliminate

$$Q(x, E) = ax + bp(x, E) = \pm \sqrt{\frac{E - x^2}{1 - x^2}}$$

in Hamilton's equations gives

$$\dot{x} \equiv \frac{dx}{dt} = \frac{\partial H}{\partial p} = \frac{2}{b}Q(1 - x^2) = \pm \frac{2}{b}\sqrt{(E - x^2)(1 - x^2)}. \tag{34}$$

These classical solutions can be used to define local WKB solutions of the form

$$\psi_{\text{WKB}}(x) = \sqrt{\frac{2}{b|\dot{x}|}} e^{\pm ik_b S(x;E) - ik_b ax^2/2} = \frac{e^{\pm ik_b S(x;E) - ik_b ax^2/2}}{[(x^2 - E)(x^2 - 1)]^{1/4}}, \tag{35}$$

where the factor of $2/b$ is put in the prefactor simply to ease presentation, the scaled wavenumber k_b has been introduced in (19) and the action function $S(x, E)$ is defined

$$S(x, E) = \int_{x_0}^x \sqrt{\frac{u^2 - E}{u^2 - 1}} du = \int_{x_0}^x \sqrt{\frac{E - u^2}{1 - u^2}} du \tag{36}$$

for some appropriately chosen reference point x_0 . These local solutions are valid away from the turning points $x = \pm\sqrt{E}$ and the singular points $x = \pm 1$. The eigenfunctions are obtained by using connection formulae across these singular and turning points to find a single well-defined global solution, and an associated quantisation condition for associated eigenvalues [44–46]. These connection formulae are obtained from established asymptotic methods but the connection across the singular points $x = \pm 1$ is a less standard problem and treatment in direct representation conceals important physical interpretations of the boundary conditions. For this reason we take an approach that emphasises the possibility of writing these local WKB solutions in alternative representations.

Each local solution of the form (35) is defined, up to a phase factor, by (a branch of) a contour of $H = E$ and a density on it, whose square root provides the amplitude [43]. For (35) this density is $\rho(x) = 2/(b|\dot{x}|)$. Transformation to a new representation, such as $\varphi(Q)$, can be shown within leading semiclassical approximation to be achieved by rewriting the density as projection onto the alternative coordinate Q and replacing the exponent by the alternative action integral

$$\int_{x_0}^x p dx \rightarrow \int_{Q_0}^Q P dQ.$$

For the most general transformation in (17), these alternative representations of the local WKB solutions in (35) are found to be of the form

$$\varphi_{\text{WKB}}(Q) = \frac{e^{\mp ik_b S(Q;E) + ik_b dx^2/2}}{[(Q^2 - E)(Q^2 - 1)]^{1/4}}, \tag{37}$$

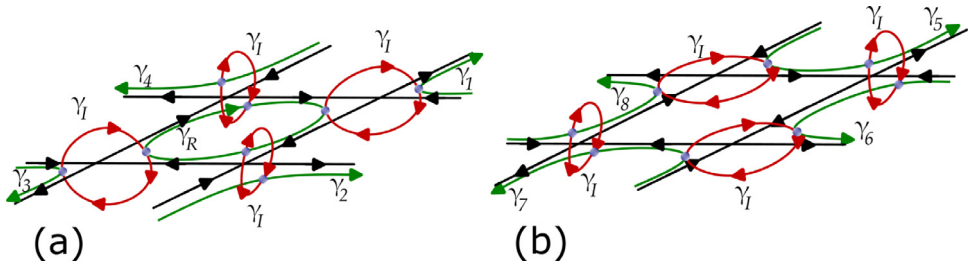


Fig. 4. The real and complex orbits used to construct local WKB solutions, are illustrated for $E < 1$ in part (a) and for $E > 1$ in part (b).

where $S(Q, E)$ is as defined in (36) except for a possible relabelling of the reference point. Swapping between alternative representations provides a simpler means of treating connection formulae across the singular points $x = \pm 1$ particularly. A detailed discussion requires us to enumerate all of the local branches forming the single global solution, which we describe next.

5.2. Real and complex orbits

We now enumerate and label the classical solutions of (27), real and complex, which are needed to build a single-valued, global eigenfunction. These solutions can be written explicitly in terms of elliptic functions as set out in Appendix B, but here in the main text we confine our attention to labelling the main topologically distinct orbits.

Let us begin with the case $0 < E < 1$. Then there is a periodic orbit, which we denote γ_R , that is confined within the parallelogram $(x, Q) \in (-1, 1) \times (-1, 1)$: see Fig. 4(a). Denote the period and action of γ_R by

$$T_R = \oint_{\gamma_R} dt \quad \text{and} \quad S_R(E) = \oint_{\gamma_R} p dx = 4S_0(E)$$

respectively, where the last equality defines $S_0(E)$. There are four further real orbits, which we denote $\gamma_1 \dots \gamma_4$, lying outside the parallelogram, one in each quadrant. In fact, with a deformation of the integration contour in the complex time plane to avoid poles, these form segments of a single periodic orbit – see Appendix B – and in fact can be deformed into γ_R . In particular, although these orbits escape to infinity, they have finite times of flight, given by

$$\int_{\gamma_1} dt = \dots = \int_{\gamma_4} dt = \frac{T_R}{4}.$$

In particular, these finite times of flight mean that corresponding WKB solutions are normalisable and can be part of a normalisable global solution, even though the classical motion is unbound. The corresponding local WKB solutions are then normalised so that

$$\begin{aligned} \int_{\gamma_i} |\psi_{\text{WKB}}(x)|^2 dx &= \frac{1}{4} \int_{\gamma_R} |\psi_{\text{WKB}}(x)|^2 dx \\ &= \frac{1}{4} \int_{\gamma_R} |\varphi_{\text{WKB}}(Q)|^2 dQ = \int_{\gamma_i} |\varphi_{\text{WKB}}(Q)|^2 dQ \end{aligned} \tag{38}$$

for $i = 1 \dots 4$.

Coupling between the WKB solutions localised on γ_R and those localised on $\gamma_1 \dots \gamma_4$ is mediated by tunnelling across a complex periodic orbit which we denote γ_I . Let the corresponding (imaginary) period and action be denoted

$$T_I = -i\tau_I \quad \text{and} \quad S_I(E) = \oint_{\gamma_I} p dx = 2iS_1(E),$$

where the last equality defines $S_1(E)$. Starting on γ_R , evolution in imaginary time ends after a half-period $T_1/2$ on one of the orbits $\gamma_1 \cdots \gamma_4$, which one depending on where on γ_R the initial condition is chosen. The relevant parameters T_1 and S_1 are independent of this choice and we use γ_1 to denote the complex periodic orbit regardless of which initial condition is used.

The periodic orbits γ_R and γ_1 can be extended to $E > 1$, defining continuous extensions of the actions $S_R(E)$ and $S_1(E)$. The complex orbit γ_1 is extended straightforwardly, for example by starting at any real initial condition in $x \in (-1, 1)$ and letting time evolve in the imaginary direction in the complex plane. There is no single closed orbit equivalent to γ_R for $E > 1$, which is replaced by partial traversal of the open orbits $\gamma_5 \cdots \gamma_8$ illustrated in Fig. 4(b). Evolution from a real initial condition in $x \in (-1, 1)$ and in real time defines an orbit which encounters poles in the Q coordinate, passing from γ_5 to γ_7 and then back to γ_5 again. From this representation we find that

$$\int_{\gamma_5} dt = \cdots \int_{\gamma_8} dt = \frac{T_R}{2}.$$

for $i = 5 \cdots 8$.

Alternatively, diversion of the time contour into the complex plane allows one to avoid these poles at the expense of allowing γ_R to incorporate complex segments (whose imaginary contributions to $S_R(E)$ cancel). In the illustration of Fig. 4(b), this representation follows γ_5 partially before crossing to γ_6 along half a representation of γ_1 and then passing similarly to γ_7 to γ_8 and back to γ_5 using complex orbits for the transitions complex orbits. If the crossings of complex orbits alternate in sign of the imaginary period τ_i , then the result is an orbit of real period and action equal to the first construction. The former approach is computationally simpler (see Appendix B), but less appealing in terms of physical intuition than the latter, which is illustrated in Fig. 4(b). Either picture defines the same action $S_R(E)$ as long as the integration contours in the complex time plane are topologically equivalent in their route between poles.

5.3. Asymptotics and boundary conditions

We now impose the boundary condition (33) on the relevant local WKB approximations. To justify this, we note that the WKB approximations set out in this section are asymptotic to exact solutions, not only as $k \rightarrow \infty$, but also for fixed k as $|Q| \rightarrow \infty$ (for $\varphi_{\text{WKB}}(Q)$). Therefore, (33) cannot hold for the exact solution unless it is also satisfied by the relevant local branches of the WKB approximations.

The local solutions on the orbits $\gamma_1 \cdots \gamma_4$ (for $E < 1$) or $\gamma_5 \cdots \gamma_8$ (for $E > 1$) give the asymptotic decays

$$|\psi_{\text{WKB}}(x)| \sim \frac{1}{|x|}$$

of the direct representation as $x \rightarrow \pm\infty$, and we can similarly characterise the solution along the vertical asymptotes $x = \pm 1$ of $\gamma_1 \cdots \gamma_4$ or $\gamma_5 \cdots \gamma_8$ using the asymptotic decay

$$|\varphi_{\text{WKB}}(Q)| \sim \frac{1}{|Q|}$$

of the alternative representation as $Q \rightarrow \pm\infty$.

Since this latter condition implies that

$$\lim_{Q \rightarrow \pm\infty} Q |\varphi_{\text{WKB}}(Q)| \neq 0,$$

then boundary conditions (33) are violated if such local branches survive in the full solution. That is, there cannot in the global eigenfunction be any components corresponding to vertical segments of $\gamma_1 \cdots \gamma_4$ (for $E < 1$) or $\gamma_5 \cdots \gamma_8$ (for $E > 1$). Note that there *can* be components corresponding to the nonvertical asymptotes of $\gamma_1 \cdots \gamma_4$ or $\gamma_5 \cdots \gamma_8$ – as long as these are switched on and off by the Stokes phenomenon as the solution is continued past the neighbourhoods of the equilibria $(x, Q) = (\pm 1, \pm 1)$. This imposes an important quantisation condition as discussed in Section 5.4.

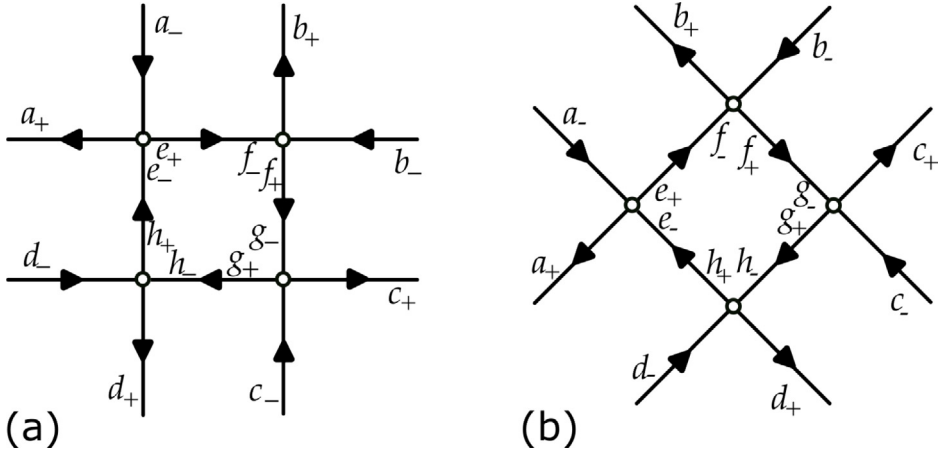


Fig. 5. Schematic representation of scattering graphs, drawn in the (x, Q) plane in part (a) and in the rotated representation of the (X, Π) plane, defined by (39), in part (b).

5.4. Quantisation

It remains to discuss how the local WKB solutions can be patched together to form a single-valued global solution consistent with connection formulae around the equilibria $(x, Q) = (\pm 1, \pm 1)$ and satisfying boundary conditions (33).

A complete solution is complicated by the fact that in each of the two natural representations $\psi(x)$ and $\varphi(Q)$ discussed so far, the orbits $\gamma_1 \cdots \gamma_4$ or $\gamma_5 \cdots \gamma_8$ have asymptotes that lead to singularities in the WKB solutions. One can patch these solutions by swapping between representations $\psi(x)$ and $\varphi(Q)$ following an asymptotic evaluation of the action of (16) (and its inverse) on them. Alternatively one can transform to a completely new representation in which none of the asymptotes have singular projections. A particularly convenient choice is to replace the transformation in (17) with $(x, p) \rightarrow (X, \Pi)$, where

$$\begin{pmatrix} X \\ \Pi \end{pmatrix} = \frac{1}{\sqrt{2b}} \begin{pmatrix} 1-a & -b \\ 1+a & b \end{pmatrix} \begin{pmatrix} x \\ p \end{pmatrix}, \tag{39}$$

which is achieved by choosing a generating function

$$F(X, x) = -\frac{1}{2}X^2 + \sqrt{\frac{2}{b}}Xx + \frac{a-1}{2b}x^2$$

to replace $F(Q, x)$ in (16). The resulting representation produces a rotated network illustrated in Fig. 5(b) which is symmetrical with respect to rotations of angle $\pi/2$ in the (X, Π) plane – for example the equilibria at $(x, Q) = (\pm 1, \pm 1)$ are moved to the axis points $(X, \Pi) = \sqrt{2/b}(\pm 1, 0)$ and $(X, \Pi) = \sqrt{2/b}(0, \pm 1)$. In particular, the asymptotes of $\gamma_1 \cdots \gamma_4$ or $\gamma_5 \cdots \gamma_8$ are not vertical. The fourfold symmetry of the network in Fig. 5(b) also simplifies the detailed treatment of the scattering problem in this section and in Appendix C.

The phase relationships between these various representations are somewhat complicated, while not being needed in detail to determine the eigenvalues λ_n , which are the primary focus of this paper. We therefore pursue a summary calculation which bypasses explicit calculation of these phases. Regardless of whether $E < 1$ or $E > 1$, the local WKB solutions form a network of the form illustrated in Fig. 5(a), with the picture obtained following the rotation (39) illustrated in Fig. 5(b). We denote the amplitudes of each of the corresponding local WKB solutions by $a_-, a_+, b_-, b_+, \dots, h_-, h_+$ as shown in Fig. 5. Amplitudes with subscript “-” describe local solutions approaching neighbourhoods of equilibria, which form nodes of the network, and amplitudes with

subscript "+" describe local solutions pointing away from them in the classical flow. The phases of these amplitudes depend on the representation being used, but the absolute values do not, as long as we normalise $\psi_{\text{WKB}}(x)$ and $\varphi_{\text{WKB}}(Q)$ consistently (so that (38) holds, for example).

We take advantage of a global symmetry of the problem with respect to the parity operation $(x, p) \rightarrow (-x, -p)$ to seek solutions that are either even or odd and so for which

$$\begin{pmatrix} a_+ \\ b_+ \end{pmatrix} = \pm \begin{pmatrix} c_+ \\ d_+ \end{pmatrix} \quad \text{and} \quad \begin{pmatrix} e_+ \\ f_+ \end{pmatrix} = \pm \begin{pmatrix} g_+ \\ h_+ \end{pmatrix} \tag{40}$$

(and similarly for incoming amplitudes a_-, b_-, \dots, h_-). We use

$$\sigma = \pm 1$$

to label the corresponding symmetry classes and beware the difference between the \pm arising in this context and the \pm used to label incoming and outgoing amplitudes.

Denote

$$\psi_{\pm} = \begin{pmatrix} a_{\pm} \\ b_{\pm} \end{pmatrix},$$

representing the amplitudes on branches of the network extending to infinity in either x or Q . Then it is shown in Appendix C that the amplitudes (e_{\pm}, f_{\pm}) on the inner, finite branches of the network can be eliminated from an imposition of consistency with respect to connection formulae at nodes to give a scattering relation of the form

$$\psi_+ = V(E)\psi_-, \tag{41}$$

where $V(E)$ is a 2×2 scattering matrix depending on actions of real and complex orbits defined in Section 5.2 (and therefore depending on E). This scattering problem does not in isolation lead to quantisation of E . Quantisation only emerges once we impose the boundary conditions in (33), which in turn impose the following conditions on the scattering amplitudes:

$$a_- = b_+ = d_+ = c_- = 0. \tag{42}$$

These conditions require that the diagonal entries in $V(E)$ should vanish, which provides a quantisation condition for E . That is, scattering should be transparent at quantisation with respect to conversion between left-right and up-down branches of the network shown in Fig. 5(a).

A detailed calculation of the scattering matrix $V(E)$ is provided in Appendix C for the rotated presentation illustrated in Fig. 5(b) (so that a single representation suffices to define nonsingular local WKB solutions along all 8 asymptotes of the network). It is shown there that the imposed boundary conditions lead to the quantisation condition

$$kS_R(E) = 4k_b S_0(E) = 2\pi \left(n + \frac{1}{2} \right) + 4\delta(E), \quad n = 0, 1, 2, \dots, \tag{43}$$

with symmetry classes

$$\sigma = (-1)^n$$

and where

$$\delta = \frac{\Theta}{\pi} \log \left| \frac{\Theta}{\pi e} \right| + \arg \left(\Gamma \left(\frac{1}{2} - i \frac{\Theta}{\pi} \right) \right) \tag{44}$$

and

$$\Theta = k_b S_1(E) \tag{45}$$

is half the imaginary action of the complex periodic orbit γ_1 defined in Section 5.2, scaled by k_b . Note that our conventions are such that $\Theta > 0$ when $0 < E < 1$ and $\Theta < 0$ when $E > 1$, while δ is an odd function of Θ .

The quantisation condition (43) is well established for the conventional problem with $Q = p$ and has been derived in detail in [44], for example. It approaches a standard Bohr-Sommerfeld

condition [39] for $0 < E < E_0$ as $k \rightarrow \infty$, where E_0 is any constant such that $E_0 < 1$, for which $\delta \rightarrow 0$. In fact, the complete quantisation condition with δ -correction is very close to quantisation conditions that arise in quantum-tunnelling problems near transitional energies (analogous to $E \rightarrow 1$ in the current problem) [47–51]. The Bohr–Sommerfeld-like quantisation condition then superficially suggests interpretation as a resonance condition of the scattering problem defined by $V(E)$. This interpretation would be misleading however, especially as E crosses the critical value $E = 1$ into the regime $E > 1$, where any resonances of the scattering problem are short-lived and do not define real energy levels even approximately. By contrast, even for $E > 1$, the quantisation condition (43) gives sharply-defined real solutions $E = E_n$ that are consequences of the boundary conditions (33) and not automatic features of the analogue quantum scattering problem.

6. Eigenvalues λ_n as tunnelling probabilities

In the previous section we have discussed semiclassical approximation of the eigenfunctions $\psi_n(x)$ and given quantisation conditions to approximate the eigenvalues E_n of the differential operator \hat{H} . We now discuss corresponding approximation of the eigenvalues λ_n of the integral operator \hat{K} . We show that they take the form of a transition probability between branches of the network shown in Fig. 5, which becomes a tunnelling probability when $E_n > 1$. These tunnelling probabilities reproduce previously established approximations of λ_n in the transition region $E_n \approx 1$, but extend them to apply universally, regardless of the value of E_n .

6.1. The main result

The basis for our derivation is a generalisation of (12) to the skewed analogue

$$\hat{T} : \psi_n(x) \mapsto \varphi_n(Q) = \frac{i^n}{\sqrt{\lambda_n}} \chi(Q) \psi_n(Q), \tag{46}$$

and can be derived from it by letting $\psi_n(x)$ be an appropriate gauge transformation of the PSWFs used in the conventional case, for example. In the network scattering picture of Fig. 5, this requires in particular that

$$\lambda_n \approx \left| \frac{e_+}{f_+} \right|^2 = \left| \frac{e_+}{h_+} \right|^2 = \left| \frac{e_+}{e_-} \right|^2. \tag{47}$$

In contrast to the interpretation of eigenvalues E_n of \hat{H} in simple physical terms as the values of the function $H(x, p)$ on quantised level sets, the use of (46) and (47) to evaluate eigenvalues λ_n of \hat{K} is rather technical: the interpretation offered below is for now presented as a mathematical equivalence rather than one with a clear intuitive motivation.

By writing the relationship (47) using absolute values of the amplitudes of WKB states, it becomes true regardless of the representation used for the network scattering problem, as long as the WKB states are normalised consistently, and so in particular applies to the amplitudes calculated in Appendix C. The rightmost equality also allows us to interpret λ_n as a transition probability for waves approaching a node of the network along a finite bond approaching it (with amplitude e_-) and scattering into a finite bond leaving it (with amplitude e_+). When $E_n > 1$, this is a tunnelling probability for a classically forbidden process for which we can use well-established semiclassical approximations [22,23,47].

As illustrated in Fig. 6, this local scattering problem is equivalent to a problem of reflection of a wave from a generic potential barrier in quantum mechanics, with $E_n < 1$ corresponding to the case of below-barrier reflection and $E_n > 1$ to above-barrier reflection. The resulting approximation

$$\lambda_n \approx \lambda_n^{\text{TUNNEL}} \equiv \frac{1}{1 + e^{-2\vartheta(E_n)}}, \tag{48}$$

where $\vartheta(E)$ has been defined in (45), emerges explicitly from the detailed calculation in Appendix C. The interpretation as a simple transition probability, coming from the rightmost equality in (47),

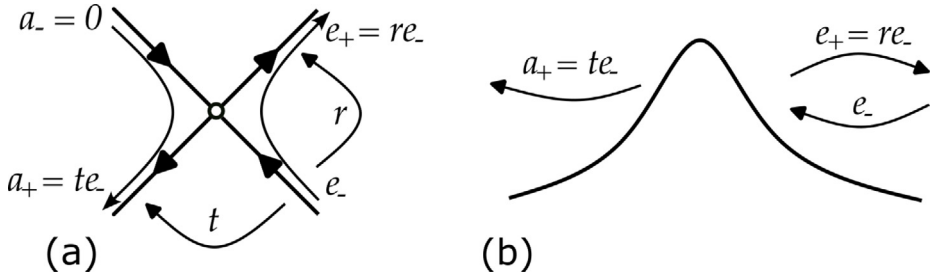


Fig. 6. The local scattering problem about a single node of the network in phase space illustrated in part (a) is analogous to the barrier-crossing problem in quantum mechanics illustrated in part (b).

allows us to make a condensed argument for the result, however, which we present in the main text.

Here we isolate the subproblem of a wave component corresponding to amplitude e_- scattering from a node it approaches and into the outgoing component e_+ , and present it as a simple barrier-penetration problem in quantum mechanics: see Fig. 6. When the condition $a_- = 0$ is satisfied (which is the case at $E = E_n$), then it corresponds in the quantum analogue to scattering of a wave being incident from the right (with no component incident from the left). The reflection and transmission coefficients for such an incident wave, as discussed in more detail in Appendix C, are in WKB approximation [22,47,49,50]

$$r = \frac{-ie^{-i\delta}}{\sqrt{1 + e^{-2\Theta}}} \quad \text{and} \quad t = \frac{e^{-i\delta}e^{-\Theta}}{\sqrt{1 + e^{-2\Theta}}}. \tag{49}$$

Then according to the rightmost equality in (47) we have

$$\lambda_n^{\text{TUNNEL}} = |r(E = E_n)|^2,$$

which gives (48). When $E_n < 1$ the reflection and transmission coefficients correspond to a below-barrier quantum tunnelling problem, with incoming amplitudes being predominantly reflected and with comparatively weak transmission across the barrier ($t \approx 0$). When $E_n > 1$ the problem transitions into an above-barrier quantum tunnelling problem, in which transmission dominates and there is comparatively weak reflection ($r \approx 0$).

6.2. Comparison with classical results

Eq. (48) generalises an established approximation [6]

$$\lambda_n \approx \lambda_n^{\text{SLEPIAN}} \equiv \frac{1}{1 + e^{\pi k(E_n - 1)/2}} \tag{50}$$

that applies around the transition at $E_n \approx 1$, extending it to apply for arbitrary E_n (in a semiclassical limit $k \rightarrow \infty$ and assuming n is large enough that WKB approximation of the eigenfunctions is appropriate). This is obtained by substituting the approximation

$$\Theta(E) = kS_1(E) = \frac{\pi k}{4}(1 - E) + O((E - 1)^2)$$

in the exponent in (48) for the case $b = 1$ (which is assumed throughout this section).

It has been shown by Widom [25] that, for fixed k and as $n \rightarrow \infty$ (so in particular $E_n \gg 1$),

$$\lambda_n \approx \lambda_n^{\text{WIDOM}} \equiv \left(\frac{ek}{2(2n + 1)} \right)^{2n+1},$$

while Fuchs has shown [24], for fixed n and as $k \rightarrow \infty$ (so in particular $E_n \ll 1$), that

$$1 - \lambda_n \simeq 1 - \lambda_n^{\text{FUCHS}} \equiv \frac{4\sqrt{\pi} 2^{3n} k^{n+1/2} e^{-2k}}{n!}.$$

The Widom approximation has more recently been improved by Bonami and Karoui [26]. We note that these approximations are restricted to particular ranges of the variable E ($E < 1$ for λ_n^{FUCHS} , $E \approx 1$ for $\lambda_n^{\text{SLEPIAN}}$ and $E > 1$ for λ_n^{WIDOM}), whereas the result in (48) spans all three regimes. Its physical interpretation as a tunnelling probability is also advantageous in making it simple to evaluate and in promising generalisation to problems such as those arising from deformed parallelograms.

We obtain the Widom approximation directly from (48) by noting that in the limit $E_n \rightarrow \infty$ the quantisation condition (43) yields (recall that $\delta \rightarrow 0$ in this limit)

$$2n + 1 \simeq \frac{4k}{\pi} S_0(E_n) \simeq 2k\sqrt{E_n}$$

(which uses the asymptotic form $S_0(E) \simeq \pi\sqrt{E}/2$ of the integral defining $S_0(E)$ for the case $E > 1$ in Appendix B), so that

$$-\frac{1}{2k} \log(\lambda_n^{\text{WIDOM}}) \simeq \sqrt{E_n} \log\left(\frac{4\sqrt{E_n}}{e}\right).$$

This is seen to be consistent with

$$-\frac{1}{2k} \log(\lambda_n^{\text{TUNNEL}}) \simeq -\frac{1}{k} \Theta = -S_1(E_n)$$

on substitution of

$$S_1(E) \simeq -\sqrt{E} \log\left(\frac{4\sqrt{E}}{e}\right),$$

which can be obtained from approximation of the explicit integral form of $S_1(E)$ given for $E > 1$ in Appendix B.

From (48) we can also reproduce a version of the Fuchs approximation in which the following modification of Stirling's approximation

$$n! \simeq \sqrt{2\pi} \left(n + \frac{1}{2}\right)^{n+1/2} e^{-(n+1/2)}$$

is substituted in it, leading to

$$\begin{aligned} -\frac{1}{2k} \log(1 - \lambda_n^{\text{FUCHS}}) &\simeq 1 + \left(\frac{n + 1/2}{2k}\right) \log\left(\frac{n + 1/2}{8ke}\right) \\ &\simeq 1 + \frac{1}{\pi} S_0(E_n) \log\left(\frac{S_0(E_n)}{4\pi e}\right), \end{aligned}$$

where the second line is obtained on using the quantisation condition (43). This approximation is reproduced by (48), which can be written

$$-\frac{1}{2k} \log(1 - \lambda_n^{\text{TUNNEL}}) = \frac{1}{k} \Theta(E_n) = S_1(E_n)$$

on substituting the following approximations of the actions

$$S_0(E) \simeq \frac{\pi E}{4} \quad \text{and} \quad S_1(E) \simeq 1 + \frac{E}{4} \log\left(\frac{E}{16e}\right),$$

which can be derived from the explicit integrals in Appendix B on taking the limit $E \rightarrow 0$. We reiterate that (48) deviates from the Fuchs approximation most significantly for small n due to the replacement of $n!$ by the Stirling approximation. This deviation is to be expected because WKB

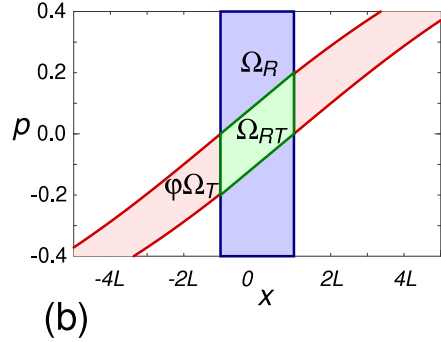
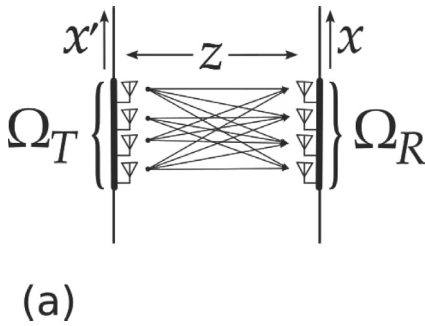


Fig. 7. In part (a) we illustrate the 2D MIMO model used as a basis for the numerical calculations in this section. In part (b) is shown the corresponding patch defined in the phase plane of the receiving boundary, with the full nonlinear dynamics shown as red curves, the strip defined by the receiving region Ω_R shaded purple and the parallelogram defined by the linearised dynamics shaded green: here we choose $L_T = L_R = L = z/5$.

approximation of the inner part of the eigenfunction assumes n is large (although the quantisation condition (43) is valid even for small n). It is known how to correct tunnelling rates to account for the form of the eigenfunction with low quantum numbers [52]: such calculations can, for example, account for the relative factor of $\sqrt{\pi/e}$ in the comparison above that arises from replacing $n!$ by its Stirling approximation when $n = 0$. A more complete connection between (48) is therefore certainly possible but we do not pursue that calculation here.

7. Application to MIMO systems

We now provide a numerical illustration of the results derived in this paper, using an idealised model of MIMO communication as motivation.

7.1. A model holographic surface problem

Consider the idealised model of MIMO communication illustrated in Fig. 7(a). In this 2D model we suppose dense arrays of transmitting and receiving antennae distributed along intervals $\Omega_T = \{-L_T/2 < x' < L_T/2\}$ and $\Omega_R = \{-L_R/2 < x < L_R/2\}$, of lengths L_T and L_R respectively, and directly opposed at a distance z apart. A ray leaving a point x' in Ω_T with momentum $p = \sin \alpha$ arrives at Ω_R at position

$$x = x' + z \tan \alpha = x' + \frac{zp}{\sqrt{1 - p^2}}.$$

Then the image $\varphi\Omega_T$ of the transmitting interval Ω_T is bounded in the phase plane of the receiving line by the curves

$$x = \pm \frac{L_T}{2} + \frac{zp}{\sqrt{1 - p^2}}, \tag{51}$$

which are illustrated in red in Fig. 7(b). The patch Ω_{RT} is the region bounded by these two curves and the bounds $x = \pm L_R/2$ of the receiving interval.

An interesting future generalisation of this work will be to calculate the analogues of Slepian eigenvalues defined by the region $\Omega_{RT} = \Omega_R \cap \varphi\Omega_T$, while accounting for the nonlinear nature of the bounds in (51). Here we consider a simpler calculation in which the nonlinear bounds (51) are replaced by the linearised versions

$$x = \pm \frac{L_T}{2} + zp.$$

If z is significantly larger than $L_{T,R}$ these limits define a parallelogram that approximates the exact region Ω_{RT} , as illustrated by patch shaded green in Fig. 7(b) for an example in which $z/L_T = z/L_R = 5$. This linearised setting places us in the context of the calculations in this paper.

To complete the connection, we define a coordinate

$$Q = -x + zp,$$

on the phase plane of the receiving antennae. Note that $-Q$ is the coordinate x' of a ray as it leaves Ω_T on its way to (x, p) : the sign is chosen so that the parameter $b = z$ defined in the notation of Section 3.4 is positive, so that we conform to the conventions set out there. Then the results of Section 6 apply on replacing

$$k \rightarrow k_{\text{eff}} \equiv \frac{\Delta Q \Delta x k_b}{4} = \frac{k L_T L_R}{4z}$$

to account for scaling of the intersection region from the conventional special case $\Delta Q = \Delta x = 2$ (see the discussion at the end of Section 3.1).

7.2. Numerical illustration

We now apply the approximations of Section 6 to the geometry illustrated in Fig. 7 (in which $z = 5L_T = 5L_R$). To compare the various approximations of λ_n with numerical results, we are motivated by (43) to define the function of energy

$$n(E) = \frac{1}{2\pi} (k_{\text{eff}} S_R(E) - 4\delta(E)) - \frac{1}{2},$$

which should take approximately integer values $n(E_n) \approx n$ when E_n is an eigenvalue of \hat{H} . We also denote the value at the critical energy $E = 1$ by

$$N_{\text{max}} = n(1) = \frac{2k_{\text{eff}}}{\pi} - \frac{1}{2}$$

(note that $S_R(1) = 4$ and $\delta(1) = 0$). For the purposes of comparison we also define the quantity

$$\Delta\lambda_n = \begin{cases} 1 - \lambda_n & E_n < 1 \\ \lambda_n & E_n > 1, \end{cases}$$

which is small except in the transition region $E_n \approx 1$.

We plot each of the various approximations for λ_n as parametrised curves $(n(E), \lambda^{\text{APPROX}}(E))$ for $k_{\text{eff}} = 5\pi/2$ in Fig. 8, where APPROX is one of TUNNEL, SLEPIAN, FUCHS or WIDOM (the integer n in the Fuchs approximation is replaced by $n(E)$ here in order to present it as a continuous curve). We also show numerically calculated values of λ_n (obtained using the expansion in Legendre Polynomials described in [11]), plotted against n for the values $n = 0, 2, 4 \dots$. Although the chosen value of k_{eff} is not particularly large (it corresponds to $N_{\text{max}} = 9/2$), these eigenvalues λ_n lie approximately on the curves for the various approximations within their domains of validity. Furthermore, the result (48) applies across all these regimes, successfully interpolating between the domains of validity of Fuchs to Slepian to Widom. The relative sizes of the various approximations and the numerical evaluation are further exemplified in Fig. 9, where the ratio $\Delta\lambda_n / \Delta\lambda_n^{\text{TUNNEL}}$ is plotted, with the parameter values of Fig. 8 being shown in part (a) and a separate calculation for the larger values $k_{\text{eff}} = 5\pi$ and $N_{\text{max}} = 19/2$ being shown in part (b). The use of a linear scale helps to highlight the greater overall accuracy of (48). Except for the first eigenvalue, we find in these examples that the tunnelling model performs at least as well as, and often considerably better than, each of the classical approximations: the better accuracy of the Fuchs approximation for the lowest eigenvalues is expected, as discussed at the end of Section 6.2.

The exponential approach of eigenvalues λ_n to 1 or 0 outside of the window where the Slepian approximation is valid means that in practice the wider validity of our tunnelling model will be of limited importance to global measures of communication rates such as the channel capacity defined in Section 2.1. We note, however, that there is additional information available in the more complete results, for example, the fall-off in individual channel strengths outside of the set supported inside the patch Ω_{RT} .

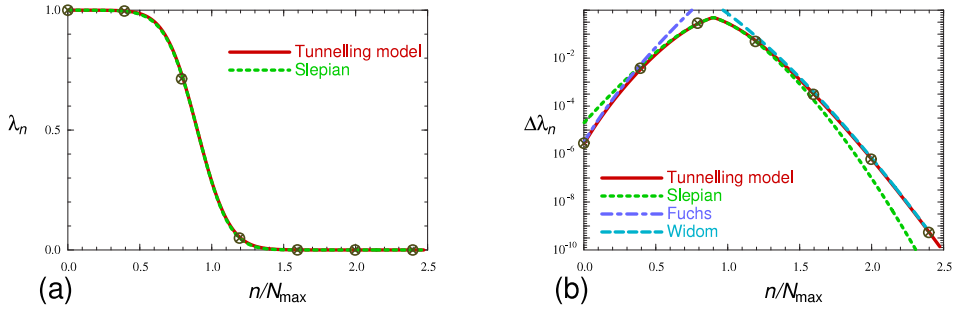


Fig. 8. In part (a) we show in red the curve defined by $(n(E), \lambda_n^{\text{TUNNEL}}(E))$ (parametrised by E) along with the first few values of (n, λ_n) , shown as crossed circles, computed numerically for even values of n with $k_{\text{eff}} = 5\pi/2$ (so $N_{\text{max}} = 9/2$). This agrees well with the approximation (50), presented as a green-dashed curve which applies over the transition region. In part (b) we compare numerically-computed values of $\Delta\lambda_n$ with corresponding approximations by Fuchs (for $E_n < 1$), by Slepian (for $E_n \approx 1$) by Widom (for $E_n > 1$) and by (48) (for all E_n). Here we see that (50) in particular deviates significantly outside of the transition region, whereas (48) does not.

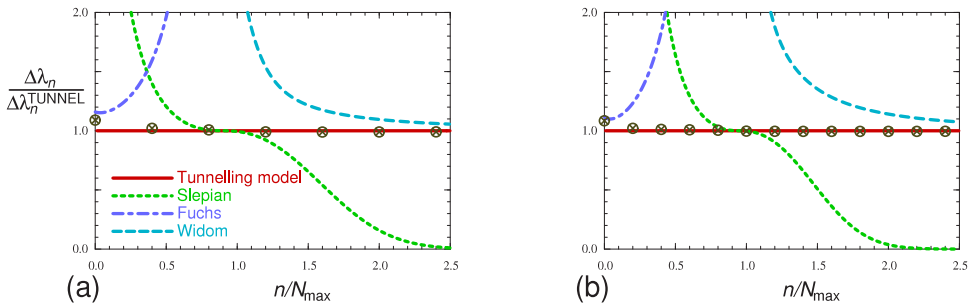


Fig. 9. The ratios of $\Delta\lambda_n$ to the values $\Delta\lambda_n^{\text{TUNNEL}}$ predicted by (48) are shown on a linear scale. The plot in part (a) uses the same parameters as in Fig. 8 (so in particular $k_{\text{eff}} = 5\pi/2$ and $N_{\text{max}} = 9/2$). We add an equivalent comparison in part (b) for the larger values $k_{\text{eff}} = 5\pi$ and $N_{\text{max}} = 19/2$. Of course, the red curves corresponding to the tunnelling model are trivial in these plots but are included to ease comparison. After the first couple of eigenvalues, where the differences are visually apparent, the relative error of the tunnelling model falls to about a percent in part (a) and about half a percent in part (b). Note that to achieve this accuracy, we use the semiclassical approximation of E_n when evaluating (48) to scale the numerically calculated eigenvalues: the errors are significantly larger if this is evaluated using the exact value of E_n .

8. Conclusion

We have expressed the eigenvalues of the integral operator in (1) as transition probabilities in an analogue quantum problem. This allows us to approximate the eigenvalues using well-established approaches to quantum tunnelling using real and complex orbits of a corresponding classical Hamiltonian. These approximations extend the range of validity of a well-known approximation of the eigenvalues given by Slepian previously, approaching it in the transition region where the eigenvalues pass from being near unity to near zero. This single result uniformly extends Slepian’s approximation so that it interpolates between regimes where distinct approximations have been provided by Fuchs and Widom.

The integral operator (1) has been studied primarily for its role in signal processing but is developing a new relevance in the context of radio communication by MIMO arrays. Here however, more general forms are relevant where filtering in the Fourier domain is by more general windows than in the signal processing context. The tunnelling picture presented in this paper is promising as an approach in this more general setting, and has been explicitly applied to skewed geometries where the relevant phase space region is a parallelogram rather than a rectangle. It also points to

a generalisation to more general regions defined by curvilinear boundaries, albeit at the expense of replacing previously exact symmetries (commutation with the Hamiltonian \hat{H}) with approximate ones. We will show in a future publication that the eigenvalues in this more general case still lie on the parametrised curves exemplified in Fig. 8, with the simple modification that the value of the parameter $k_{\text{eff}} = kA/4$ is adjusted to account for the area A in phase space of the deformed patch.

CRedit authorship contribution statement

Stephen C. Creagh: Conceptualization, Methodology, Software, Formal analysis, Writing – original draft, Visualization. **Gabriele Gradoni:** Conceptualization, Methodology, Writing – review & editing, Funding acquisition.

Declaration of competing interest

The authors declare that they have no known competing financial interests or personal relationships that could have appeared to influence the work reported in this paper.

Data availability

Data will be made available on request.

Acknowledgements

We are grateful to Gregor Tanner for helpful discussions, especially on the incorporation of boundary conditions in the quantisation of graph scattering models. This work is supported by EU H2020 RISE-6G project, grant number 101017011, and by Royal Society Industry Fellowship, UK, grant number INF\R2\192066.

Appendix A. Boundary conditions for flux conservation

In this Appendix we motivate further the boundary conditions imposed on eigenfunctions in Section 4.3. Let a prime signify the following scaled commutator

$$[\hat{A}, \hat{B}]' \equiv -ik_b[\hat{A}, \hat{B}]$$

of operators \hat{A} and \hat{B} , where $k_b = k/b$ is the scaled wavenumber introduced in Section 3.4. Then

$$[\hat{x}, \hat{Q}]' = \hat{I},$$

where \hat{I} is the identity operator and, furthermore,

$$[\hat{x}, f(\hat{Q})]' = f'(\hat{Q}),$$

and

$$[g(\hat{x}), \hat{Q}]' = g'(\hat{x}), \tag{A.1}$$

are well-established identities in quantum mechanics, where $g(\hat{x})$ denotes an operator defined by

$$g(\hat{x})\psi(x) = g(x)\psi(x)$$

for any function $g(x)$, $g'(x)$ denotes its derivative and the operator $f(\hat{Q})$ is defined analogously by its action

$$f(\hat{Q})\psi(x) = \hat{T}^{-1} [f(Q)\varphi(Q)]$$

on the integral transform $\varphi(Q)$. Within this convention we can also denote

$$\hat{L} = \chi(\hat{x}) \quad \text{and} \quad \hat{M} = \chi(\hat{Q})$$

and for convenience we will also interchangeably write

$$g(\hat{x}) = g(x) = g(x)\hat{I}$$

where there is no risk of confusion. We will also make repeated use of the derivation identity

$$[\hat{A}, \hat{B}\hat{C}] = [\hat{A}, \hat{B}]\hat{C} + \hat{B}[\hat{A}, \hat{C}] \tag{A.2}$$

in the following.

Let us first establish the conditions under which the identity

$$[\hat{L}, \hat{H}] = 0$$

holds. Since $\hat{L} = \chi(\hat{x})$ is a function of \hat{x} , we trivially find

$$[\hat{L}, \hat{x}] = 0,$$

while

$$[\hat{L}, \hat{Q}]' = \chi'(x)$$

is a special case of (A.1). Note that $\chi'(x)$ (and any further derivatives to be encountered below) is distributionally concentrated on $x = \pm 1$, so the action of this last commutator (or whether its action is defined in the first place) will depend on the boundary conditions imposed at these singular points. By repeated application of (A.2) we can also establish that

$$\begin{aligned} [\hat{L}, \hat{Q}^2]' &= \chi'(x)\hat{Q} + \hat{Q}\chi'(x) \\ &= 2\chi'(x)\hat{Q} + [\hat{Q}, \chi'(x)] \\ &= 2\chi'(x)\hat{Q} - \frac{i}{k_b}\chi''(x) \end{aligned}$$

and by a similar calculation that

$$[\hat{L}, \hat{x}\hat{Q}^2\hat{x}]' = 2x^2\chi'(x)\hat{p} - 2\frac{i}{k_b}x\chi'(x) - \frac{i}{k_b}x^2\chi''(x).$$

Combined with (26) this provides the formal identity

$$[\hat{L}, \hat{H}]' = 2(1 - x^2)\chi'(x)\hat{Q} - \frac{i}{k_b}[(1 - x^2)\chi'(x)]'.$$

We must next determine boundary conditions on solutions $\psi(x)$ so that

$$[\hat{L}, \hat{H}]'\psi(x) = 0 \tag{A.3}$$

is guaranteed.

From the identity

$$\chi'(x) = \delta(x - 1) - \delta(x + 1)$$

we find that

$$(1 - x^2)\chi'(x) = 0$$

in the sense of distributions, and condition (A.3) is therefore automatically satisfied when $\psi(x)$ is taken from the usual spaces of (sufficiently smooth) test functions. However, for functions with logarithmic singularities such as the second case listed in (30), we find that

$$(1 - x^2)\hat{Q}\psi(x) \sim \text{constant as } x \rightarrow \pm 1$$

and we conclude that (A.3) fails for them. The operations in (A.3) are well defined on the other hand for continuously differentiable functions $\psi(x)$, which is the boundary condition imposed on solutions of the integral equation and associated differential equation.

Condition (A.3), and the resulting requirement to eliminate logarithmically divergent solutions, can be given a simple physical interpretation in terms of flux crossing the lines defined by $x = \pm 1$, which can be written

$$\Phi \propto \langle \psi | [\hat{L}, \hat{H}] | \psi \rangle,$$

up to a constant factor. In other words, boundary condition (A.3) makes this flux vanish, while this is not automatically the case for arbitrary solutions of the differential equation defined by (26). Flux conservation is nontrivial across $x = \pm 1$ for the Hamiltonian (26) because the classical analogue has unstable manifolds along the corresponding vertical lines in phase space, which can act as sinks diverting flux that is incident from the left or right. Solutions which include the logarithmic singularities in (30) have nonzero flux in these vertical directions and a resulting nonconservation of flux across $x = \pm 1$: this interpretation becomes more evident for the alternative form of the boundary conditions in (33), which explicitly eliminate branches of the corresponding scattering problem carrying flux in these vertical directions. This interpretation of the boundary conditions in terms of flux carried by the unstable manifold will be useful in generalising the present calculations to the case of nonlinear coordinate changes as set out in Section 3.4.

Appendix B. Real and complex orbits as elliptic functions

We now further motivate the properties of real and complex orbits of $H(x, p)$, discussed in Section 5.2, by demonstrating them to be properties of explicit solutions derived in terms of elliptic functions and integrals [41]. As in the discussion provided in the main text, it is helpful to separate these solutions into the cases $0 < E < 1$ and $E > 1$.

B.1. The case $0 < E < 1$

Integrating (34) with the initial condition $x(0) = 0$ and $\dot{x}(0) > 0$, one can show that

$$x(t) = \sqrt{E} \operatorname{sn}(2t/b|E) \quad \text{and} \quad Q(t) = \sqrt{E} \operatorname{cd}(2t/b|E), \tag{B.1}$$

where sn and cd are Jacobi elliptic functions in the notation of [41]. Note that $\operatorname{sn}(u|E)$ has real and imaginary periods $4\mathbf{K}$ and $2i\mathbf{K}'$, where

$$\mathbf{K}(E) = \int_0^{\sqrt{E}} \frac{dx}{\sqrt{(E-x^2)(1-x^2)}} \quad \text{and} \quad \mathbf{K}'(E) = \mathbf{K}(1-E)$$

denote complete elliptic integrals in the notation of [41] (we introduce a bold font to distinguish them from the operator \hat{K} and its symbol $K(x, p)$). Corresponding to the real period, the solution (B.1) therefore defines a real periodic orbit γ_R with real period $T_R = 2b\mathbf{K}(E)$. This periodic orbit has action

$$S_R(E) = \oint_{\gamma_R} p dx = \frac{1}{b} \oint_{\gamma_R} Q dx = \frac{4}{b} S_0(E), \tag{B.2}$$

where

$$S_0(E) = \int_0^{\sqrt{E}} \sqrt{\frac{E-x^2}{1-x^2}} dx = \mathbf{E}(E) - (1-E)\mathbf{K}(E)$$

and where $\mathbf{E}(E)$ denotes the complete elliptic integral of the second kind [41].

We can identify the complex periodic orbit γ_I with the imaginary period $i\mathbf{K}'(E)$ of $\operatorname{sn}(u|E)$ [41], so that $T_I = ib\mathbf{K}'(E)$. This has an imaginary action

$$S_I(E) = \oint_{\gamma_I} p dx = \frac{1}{b} \oint_{\gamma_I} Q dx = \frac{2i}{b} S_1(E), \tag{B.3}$$

where

$$S_1(E) = \int_{\sqrt{E}}^1 \sqrt{\frac{x^2 - E}{1 - x^2}} dx = \mathbf{E}(1 - E) - E\mathbf{K}(1 - E).$$

This imaginary action is the single most important property of the classical solutions for the purposes of this paper.

Finally, it is useful to note how the complex orbit γ_1 allows us to connect the real periodic orbit γ_R to the four outer branches $\gamma_1 \cdots \gamma_4$ of the energy contour. If we start the complex periodic orbit γ_1 at $x(0) = 0$, it runs into a pole at the half period $t = T_1/2$, but this is avoided for almost all other conditions. If (real) initial conditions other than those on the coordinate axes $x = 0$ and $Q = 0$ are chosen, then after a half period $t = T_1/2$ one returns to the real phase plane, on one of $\gamma_1 \cdots \gamma_4$. Solutions on these outer contours can be written for appropriate initial conditions as

$$x(t) = \pm ns(2t/b|E) \quad \text{and} \quad Q(t) = \pm dc(2t/b|E),$$

where all four sign combinations arise, corresponding to each of the four branches.

B.2. The case $E > 1$

For $E > 1$ the solution (B.1) is more conveniently expressed, using reciprocal parameter relations of the elliptic functions, as

$$x(t) = \text{sn}\left(2\sqrt{E}t/b\left|\frac{1}{E}\right.\right) \quad \text{and} \quad Q(t) = \sqrt{E}\text{dc}\left(2\sqrt{E}t/b\left|\frac{1}{E}\right.\right). \tag{B.4}$$

Although $x(t)$ oscillates smoothly between -1 and 1 for real t in this solution, with period

$$T_R = \frac{2b}{\sqrt{E}}\mathbf{K}\left(\frac{1}{E}\right),$$

the coordinate $Q(t)$ passes through poles at $t = bT_R/4$ and $t = 3bT_R/4$, switching sign each time. We use this extended solution γ_R to define an action once again by (B.2), but now with

$$S_0(E) = \int_0^1 \sqrt{\frac{E - x^2}{1 - x^2}} dx = \sqrt{E}\mathbf{E}\left(\frac{1}{E}\right).$$

The imaginary period

$$T_1 = \frac{b}{\sqrt{E}}\mathbf{K}\left(1 - \frac{1}{E}\right),$$

of this solution likewise defines a complex periodic orbit γ_1 with imaginary action given once again by (B.3) but now with

$$S_1(E) = - \int_1^{\sqrt{E}} \sqrt{\frac{E - x^2}{x^2 - 1}} dx = \sqrt{E}\mathbf{E}\left(1 - \frac{1}{E}\right) - \sqrt{E}\mathbf{K}\left(1 - \frac{1}{E}\right).$$

We have defined the actions of the complex periodic orbit so that the imaginary part is *positive* when $0 < E < 1$ and *negative* when $E > 1$. This convention is important for their use in approximation of tunnelling probabilities in (48). It derives from a contour encircling the branch points $x = \pm 1$ and $x = \pm\sqrt{E}$ of $p(x, E)$ in the same sense whether $E < 1$ or $E > 1$.

Finally, as with the case $0 < E < 1$, evolution for half an imaginary period maps the real solution in (B.4) into a second real solution defined on separate branches of the level contour $H(x, p) = E$ outside the central square. These can be parametrised so that

$$x(t) = \sqrt{E}\text{dc}\left(2\sqrt{E}t/b\left|\frac{1}{E}\right.\right) \quad \text{and} \quad Q(t) = \text{sn}\left(2\sqrt{E}t/b\left|\frac{1}{E}\right.\right).$$

and are rotations of the solutions in (B.4) so that now $Q(t)$ oscillates smoothly between -1 and 1 while $x(t)$ passes through a pole and changes sign every half period $T_R/2$.

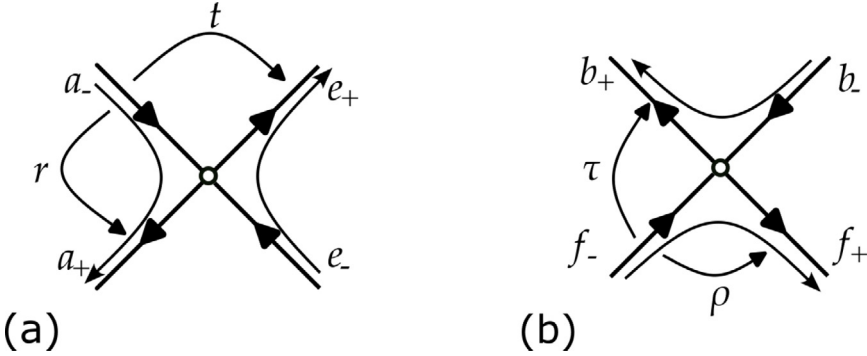


Fig. C.10. Illustration of the locally defined scattering coefficients in (C.1) (in part (a)) and (C.2) (in part (b)).

Appendix C. A scattering picture

In this appendix we find the scattering matrix $V(E)$ defined by (41) and use it to derive the quantisation condition given in (43).

C.1. Local scattering matrices

Around each node of the graph illustrated in Fig. 5(b) we define local scattering matrices as follows. Connection formulae across the nodes centred on $(x, Q) = \pm(-1, 1)$, obtained by matching solutions to the problems of waves scattering from a quadratic potential, can be written so that at leading order we have

$$\begin{pmatrix} a_+ \\ e_+ \end{pmatrix} = \begin{pmatrix} r & t \\ t & r \end{pmatrix} \begin{pmatrix} a_- \\ e_- \end{pmatrix} \quad \text{and} \quad \begin{pmatrix} c_+ \\ g_+ \end{pmatrix} = \begin{pmatrix} r & t \\ t & r \end{pmatrix} \begin{pmatrix} c_- \\ g_- \end{pmatrix}, \tag{C.1}$$

where r and t have been defined in (49) and are illustrated in Fig. C.10(a).

The nodes centred on $(x, Q) = \pm(1, 1)$ are treated similarly except that the roles of below- and above-barrier tunnelling are reversed. When $0 < E < 1$ scattering is predominantly by transmission, whereas when $E > 1$ it is predominantly by reflection. This is accounted for by changing the sign of Θ in the expressions for reflection and transmission coefficients. However, there is also a time reversal compared to conventional barrier scattering – the branch above the fixed point in phase space is right-to-left where as it is left-to-right in potential scattering. As a result we preserve the sign of δ even while reversing the sign of the imaginary action. As a result we have,

$$\begin{pmatrix} b_+ \\ f_+ \end{pmatrix} = \begin{pmatrix} \rho & \tau \\ \tau & \rho \end{pmatrix} \begin{pmatrix} b_- \\ f_- \end{pmatrix} \quad \text{and} \quad \begin{pmatrix} d_+ \\ h_+ \end{pmatrix} = \begin{pmatrix} \rho & \tau \\ \tau & \rho \end{pmatrix} \begin{pmatrix} d_- \\ h_- \end{pmatrix}, \tag{C.2}$$

where

$$\rho = ir \quad \text{and} \quad \tau = it$$

are illustrated in Fig. C.10(b) and r and t are as defined in (49).

Finally, we can connect solutions along the inner branches of the graph using

$$\begin{pmatrix} e_- \\ f_- \\ g_- \\ h_- \end{pmatrix} = \begin{pmatrix} 0 & 0 & 0 & e^{i\phi} \\ e^{i\phi} & 0 & 0 & 0 \\ 0 & e^{i\phi} & 0 & 0 \\ 0 & 0 & e^{i\phi} & 0 \end{pmatrix} \begin{pmatrix} e_+ \\ f_+ \\ g_+ \\ h_+ \end{pmatrix},$$

where

$$\Phi = k_b S_1$$

is a quarter of the phase of the real periodic orbit γ_R . For the symmetry classes in (40) these can be expressed in the reduced form

$$\begin{pmatrix} e_- \\ f_- \end{pmatrix} = \begin{pmatrix} 0 & \sigma e^{i\Phi} \\ e^{i\Phi} & 0 \end{pmatrix} \begin{pmatrix} e_+ \\ f_+ \end{pmatrix}.$$

C.2. An exterior scattering matrix

Letting

$$\psi_{\pm} = \begin{pmatrix} a_{\pm} \\ b_{\pm} \end{pmatrix} \quad \text{and} \quad \varphi_{\pm} = \begin{pmatrix} e_{\pm} \\ f_{\pm} \end{pmatrix},$$

represent the amplitudes of the inner and outer branches of the graph respectively, the previously given local scattering relations can be written as

$$\psi_+ = R\psi_- + T\varphi_-, \quad \varphi_+ = T\psi_- + R\varphi_-, \quad \varphi_- = U\varphi_+, \tag{C.3}$$

where

$$R = \begin{pmatrix} r & 0 \\ 0 & \rho \end{pmatrix}, \quad T = \begin{pmatrix} t & 0 \\ 0 & \tau \end{pmatrix}, \quad U = \begin{pmatrix} 0 & \sigma e^{i\Phi} \\ e^{i\Phi} & 0 \end{pmatrix}.$$

The inner amplitudes φ_{\pm} can then be eliminated to give (41) with [53]

$$V = R + TU \frac{1}{1 - RU} T.$$

This can be shown to be of the form

$$V = \frac{1}{\Delta} \begin{pmatrix} r(1 + \sigma i e^{2i(\Phi - \delta)}) & \sigma t \tau e^{i\Phi} \\ t \tau e^{i\Phi} & \rho(1 + \sigma i e^{2i(\Phi - \delta)}) \end{pmatrix},$$

where

$$\Delta = \det(I - RU) = 1 - \sigma i r^2 e^{2i\Phi}.$$

C.3. Quantisation

The boundary conditions (42) hold if and only if the diagonal elements of $V(E)$ vanish, so that

$$1 + \sigma i e^{2i(\Phi - \delta)} = 0.$$

This can be written in the form of the quantisation condition (43) given in the main text.

When this quantisation condition is satisfied, we find that

$$\frac{1}{\Delta} = 1 + e^{2\Theta}$$

and the outer scattering matrix reduces to the form

$$V = i^n e^{3\pi i/4 - i\delta} \begin{pmatrix} 0 & \sigma \\ 1 & 0 \end{pmatrix}.$$

We can therefore find a solution where the nonzero amplitudes on the outer branches of the graph are

$$b_- = \sigma d_- = 1, \quad a_+ = \sigma c_+ = i^n e^{3\pi i/4 - i\delta}.$$

The inner amplitudes can be found by solving (C.3) to give

$$\varphi_+ = \frac{1}{1 - RU} T \psi_-,$$

which can be shown to reduce to

$$e_+ = \sigma g_+ = \sigma e^{-2i\delta} e^{\Theta}, \quad f_+ = \sigma h_+ = i e^{-i\delta} \sqrt{1 + e^{2\Theta}}.$$

We note in particular that

$$\left| \frac{e_+}{f_+} \right|^2 = \frac{1}{1 + e^{-2\Theta}}$$

as asserted in the main text.

References

- [1] D. Slepian, H.O. Pollak, *Bell Syst. Tech. J.* 40 (1) (1961) 43–63, <http://dx.doi.org/10.1002/j.1538-7305.1961.tb03976.x>, URL: <https://onlinelibrary.wiley.com/doi/abs/10.1002/j.1538-7305.1961.tb03976.x>.
- [2] H.J. Landau, H.O. Pollak, *Bell Syst. Tech. J.* 40 (1) (1961) 65–84, <http://dx.doi.org/10.1002/j.1538-7305.1961.tb03977.x>, URL: <https://onlinelibrary.wiley.com/doi/abs/10.1002/j.1538-7305.1961.tb03977.x>.
- [3] H.J. Landau, H.O. Pollak, *Bell Syst. Tech. J.* 41 (4) (1962) 1295–1336, <http://dx.doi.org/10.1002/j.1538-7305.1962.tb03279.x>, URL: <https://onlinelibrary.wiley.com/doi/abs/10.1002/j.1538-7305.1962.tb03279.x>.
- [4] D. Slepian, *Bell Syst. Tech. J.* 43 (6) (1964) 3009–3057, <http://dx.doi.org/10.1002/j.1538-7305.1964.tb01037.x>, URL: <https://onlinelibrary.wiley.com/doi/abs/10.1002/j.1538-7305.1964.tb01037.x>.
- [5] D. Slepian, *Bell Syst. Tech. J.* 57 (5) (1978) 1371–1430, <http://dx.doi.org/10.1002/j.1538-7305.1978.tb02104.x>, URL: <https://onlinelibrary.wiley.com/doi/abs/10.1002/j.1538-7305.1978.tb02104.x>.
- [6] D. Slepian, *J. Math. Phys.* 44 (1–4) (1965) 99–140, <http://dx.doi.org/10.1002/sapm196544199>, URL: <https://onlinelibrary.wiley.com/doi/abs/10.1002/sapm196544199>.
- [7] D. Slepian, *J. Opt. Soc. Amer.* 55 (9) (1965) 1110–1115, <http://dx.doi.org/10.1364/JOSA.55.001110>, URL: <https://opg.optica.org/abstract.cfm?URI=josa-55-9-1110>.
- [8] D. Slepian, *SIAM Rev.* 25 (3) (1983) 379–393, <http://dx.doi.org/10.1137/1025078>.
- [9] F.J. Simons, *Handbook of Geomathematics*, Springer Berlin Heidelberg, 2010, pp. 891–923, http://dx.doi.org/10.1007/978-3-642-01546-5_30.
- [10] A. Osipov, V. Rokhlin, H. Xiao, et al., *Prolate Spheroidal Wave Functions of Order Zero*, Vol. 187, Springer, 2013.
- [11] L.-L. Wang, *J. Math. Study* 50 (2) (2017) 101–143.
- [12] H. Kogelnik, T. Li, *Appl. Opt.* 5 (10) (1966) 1550–1567, <http://dx.doi.org/10.1364/AO.5.001550>, URL: <https://opg.optica.org/ao/abstract.cfm?URI=ao-5-10-1550>.
- [13] P. Martinsson, P. Ma, A. Burvall, A.T. Friberg, *Optik* 119 (3) (2008) 103–111, <http://dx.doi.org/10.1016/j.ijleo.2006.07.009>, URL: <https://www.sciencedirect.com/science/article/pii/S0030402606002385>.
- [14] D.A.B. Miller, *Adv. Opt. Photon.* 11 (3) (2019) 679–825, <http://dx.doi.org/10.1364/AOP.11.000679>, URL: <https://opg.optica.org/aop/abstract.cfm?URI=aop-11-3-679>.
- [15] A. Capozzoli, C. Curcio, A. Lisenò, *Sensors* 21 (13) (2021) <http://dx.doi.org/10.3390/s21134460>, URL: <https://www.mdpi.com/1424-8220/21/13/4460>.
- [16] D.A.B. Miller, *Appl. Opt.* 39 (11) (2000) 1681–1699, <http://dx.doi.org/10.1364/AO.39.001681>, URL: <http://ao.osa.org/abstract.cfm?URI=ao-39-11-1681>.
- [17] E. Torkildson, U. Madhoo, M. Rodwell, *IEEE Trans. Wireless Commun.* 10 (12) (2011) 4150–4160, <http://dx.doi.org/10.1109/TWC.2011.092911.101843>.
- [18] M. Franceschetti, *Wave Theory of Information*, Cambridge University Press, 2017.
- [19] H. Shim, H. Chung, O.D. Miller, *Phys. Rev. A* 14 (2020) 014007, <http://dx.doi.org/10.1103/PhysRevApplied.14.014007>, URL: <https://link.aps.org/doi/10.1103/PhysRevApplied.14.014007>.
- [20] J. Ankerhold, *Quantum Tunneling in Complex Systems: The Semiclassical Approach*, Vol. 224, Springer, 2007, <http://dx.doi.org/10.1007/3-540-68076-4>, URL: <https://link.springer.com/book/10.1007/3-540-68076-4>.
- [21] S. Keshavamurthy, P. Schlagheck, *Dynamical Tunneling: Theory and Experiment*, CRC Press, 2011.
- [22] S.C. Creagh, *Nonlinearity* 18 (5) (2005) 2089–2110, <http://dx.doi.org/10.1088/0951-7715/18/5/011>.
- [23] R. Schubert, H. Waalkens, S. Wiggins, *Phys. Rev. Lett.* 96 (21) (2006) 218302.
- [24] W.H. Fuchs, *J. Math. Anal. Appl.* 9 (3) (1964) 317–330.
- [25] H. Widom, *Trans. Amer. Math. Soc.* 109 (2) (1963) 278–295.
- [26] A. Bonami, A. Karoui, *Appl. Comput. Harmon. Anal.* 42 (1) (2017) 1–20, <http://dx.doi.org/10.1016/j.acha.2015.05.003>, URL: <https://www.sciencedirect.com/science/article/pii/S106352031500086X>.
- [27] I. Daubechies, *IEEE Trans. Inform. Theory* 34 (4) (1988) 605–612.
- [28] Z. Zhang, L. Dai, *ICC 2022 - IEEE International Conference on Communications*, 2022, pp. 3287–3292, <http://dx.doi.org/10.1109/ICC45855.2022.9839220>.
- [29] E. Basar, M. Di Renzo, J. De Rosny, M. Debbah, M.-S. Alouini, R. Zhang, *IEEE Access* 7 (2019) 116753–116773, <http://dx.doi.org/10.1109/ACCESS.2019.2935192>.
- [30] C. Huang, S. Hu, G.C. Alexandropoulos, A. Zappone, C. Yuen, R. Zhang, M.D. Renzo, M. Debbah, *IEEE Wirel. Commun.* 27 (5) (2020) 118–125, <http://dx.doi.org/10.1109/MWC.001.1900534>.
- [31] Z. Zhang, L. Dai, 2021, arXiv preprint [arXiv:2111.08630](https://arxiv.org/abs/2111.08630).

- [32] O.T. Demir, E. Bjornson, L. Sanguinetti, *IEEE Wirel. Commun. Lett.* 11 (5) (2022) 997–1001, <http://dx.doi.org/10.1109/LWC.2022.3152600>.
- [33] D. Dardari, *IEEE J. Sel. Areas Commun.* 38 (11) (2020) 2526–2537, <http://dx.doi.org/10.1109/JSAC.2020.3007036>.
- [34] M. Chafii, L. Bariah, S. Muhaidat, M. Debbah, 2022, arXiv preprint [arXiv:2207.01843](https://arxiv.org/abs/2207.01843).
- [35] E.C. Strinati, G.C. Alexandropoulos, V. Sciancalepore, M. Di Renzo, H. Wymeersch, D.-T. Phan-Huy, M. Crozzoli, R. D'Errico, E. De Carvalho, P. Popovski, P. Di Lorenzo, L. Bastianelli, M. Belouar, J.E. Mascolo, G. Gradoni, S. Phang, G. Lerosey, B. Denis, 2021 Joint European Conference on Networks and Communications and 6G Summit, EuCNC/6G Summit, 2021, pp. 562–567, <http://dx.doi.org/10.1109/EuCNC/6GSummit51104.2021.9482474>.
- [36] A. Mezghani, J.A. Nossek, *Proc. IEEE Int. Symp. Inf. Theory*, 2012, pp. 1–5.
- [37] A. Pizzo, L. Sanguinetti, T.L. Marzetta, *IEEE Trans. Wireless Commun.* 21 (9) (2022) 6890–6905, <http://dx.doi.org/10.1109/TWC.2022.3152965>.
- [38] A. Pizzo, A.d.J. Torres, L. Sanguinetti, T.L. Marzetta, *IEEE Trans. Signal Process.* 70 (2022) 3935–3947, <http://dx.doi.org/10.1109/TSP.2022.3183445>.
- [39] F. Haake, *Quantum Coherence in Mesoscopic Systems*, Springer, 1991, pp. 583–595.
- [40] E.B. Bogomolny, *Nonlinearity* 5 (4) (1992) 805.
- [41] M. Abramowitz, I.A. Stegun, R.H. Romer, *Handbook of Mathematical Functions with Formulas, Graphs, and Mathematical Tables*, American Association of Physics Teachers, 1988.
- [42] R.G. Littlejohn, *Phys. Rep.* 138 (4–5) (1986) 193–291.
- [43] R.G. Littlejohn, *J. Stat. Phys.* 68 (1) (1992) 7–50.
- [44] J.d. Cloizeaux, M. Mehta, *J. Math. Phys.* 13 (11) (1972) 1745–1754.
- [45] W. Boyd, T. Dunster, *SIAM J. Math. Anal.* 17 (2) (1986) 422–450.
- [46] F. Fauvet, J.-P. Ramis, F. Richard-Jung, J. Thomann, *Appl. Numer. Math.* 60 (12) (2010) 1309–1319.
- [47] K.W. Ford, J.A. Wheeler, *Ann. Physics* 7 (3) (1959) 259–286, [http://dx.doi.org/10.1016/0003-4916\(59\)90026-0](http://dx.doi.org/10.1016/0003-4916(59)90026-0), URL: <https://www.sciencedirect.com/science/article/pii/0003491659900260>.
- [48] K.W. Ford, D.L. Hill, M. Wakano, J.A. Wheeler, *Ann. Physics* 7 (3) (1959) 239–258, [http://dx.doi.org/10.1016/0003-4916\(59\)90025-9](http://dx.doi.org/10.1016/0003-4916(59)90025-9), URL: <https://www.sciencedirect.com/science/article/pii/0003491659900259>.
- [49] W.H. Miller, *J. Chem. Phys.* 48 (4) (1968) 1651–1658, <http://dx.doi.org/10.1063/1.1668891>.
- [50] J.M. Robbins, S.C. Creagh, R.G. Littlejohn, *Phys. Rev. A* 41 (1990) 6052–6062, <http://dx.doi.org/10.1103/PhysRevA.41.6052>, URL: <https://link.aps.org/doi/10.1103/PhysRevA.41.6052>.
- [51] N.M. Mohammed, S.C. Creagh, G. Tanner, *Wave Motion* 101 (2021) 102697, <http://dx.doi.org/10.1016/j.wavemoti.2020.102697>, URL: <https://www.sciencedirect.com/science/article/pii/S0165212520303279>.
- [52] A. Garg, *Amer. J. Phys.* 68 (5) (2000) 430–437, <http://dx.doi.org/10.1119/1.19458>.
- [53] S. Gnutzmann, U. Smilansky, *Adv. Phys.* 55 (5–6) (2006) 527–625, <http://dx.doi.org/10.1080/00018730600908042>.